Lawrence Berkeley National Laboratory

Recent Work

Title

HEAVY-CHARGED-PARTICLE BEAMS.

Permalink

https://escholarship.org/uc/item/99x5d412

Authors

Raju, Mudundi R.
Lyman, John T.
Brustad, Tor
et al.

Publication Date

1968-03-01

eScholarship.org Powered by the California Digital Library
University of California

UCRL-16962 Rev.
Cy. 2

RECEIVED
LAWRENCE
RADIATION LABORATORY
OCT 25 1968
LIBRARY AND
DOCUMENTS SECTION

University of California

Ernest O. Lawrence Radiation Laboratory

TWO-WEEK LOAN COPY

This is a Library Circulating Copy which may be borrowed for two weeks. For a personal retention copy, call Tech. Info. Division, Ext. 5545

HEAVY-CHARGED-PARTICLE BEAMS

Mudundi R. Raju, John T. Lyman, Tor Brustad, and Cornelius A. Tobias

March 1968

Berkeley, California

UCRL-16962 Rev
Cy. 2

DISCLAIMER

This document was prepared as an account of work sponsored by the United States Government. While this document is believed to contain correct information, neither the United States Government nor any agency thereof, nor the Regents of the University of California, nor any of their employees, makes any warranty, express or implied, or assumes any legal responsibility for the accuracy, completeness, or usefulness of any information, apparatus, product, or process disclosed, or represents that its use would not infringe privately owned rights. Reference herein to any specific commercial product, process, or service by its trade name, trademark, manufacturer, or otherwise, does not necessarily constitute or imply its endorsement, recommendation, or favoring by the United States Government or any agency thereof, or the Regents of the University of California. The views and opinions of authors expressed herein do not necessarily state or reflect those of the United States Government or any agency thereof or the Regents of the University of California.

Chapter in book "Radiation Dosimetry"
Published by Academic Press

UCRL-16962 Rev.
Preprint

UNIVERSITY OF CALIFORNIA

Lawrence Radiation Laboratory
Berkeley, California

AEC Contract No. W-7405-eng-48

HEAVY-CHARGED-PARTICLE BEAMS

Mudundi R. Raju, John T. Lyman, Tor Brustad,
and Cornelius A. Tobias

March 1968

HEAVY-CHARGED-PARTICLE BEAMS

Contents

I. INTRODUCTION

Accelerated heavy charged particles, because of their distinct physical properties, are of interest in radiation biology and nuclear medicine. The masses of heavy charged particles are many times that of the electron, and the angle of scattering in a given collision is reduced approximately by the ratio of the masses; hence, heavy charged particles produce a more sharply defined beam than do electrons of comparable velocity, and thus undesirable side scattering can be reduced to a minimum. For this reason, the radiation field of heavy charged particles can also be shaped with greater precision than it can be for x rays and γ rays. The heavy charged-particle beam has a rather definite range of penetration depending on its energy. As the particle proceeds through a medium its rate of energy loss or relative specific ionization increases with decreasing particle velocity, giving rise to a sharp maximum in ionization known as the Bragg peak near the end of the range. These properties make possible intense irradiation of a strictly localized region within the body, with little skin dose (Tobias et al., 1952).

Various types of particle accelerators have been discussed in a review article by McMillan (1959), and Hubbard (1961) has discussed accelerators for heavy ions. A list of existing accelerator facilities throughout the world was given by Gordon and Behman (1963).

A major problem in radiation biology is the manner in which ionizing radiation exerts its biological effects. It is well known that the magnitude of these effects depends not only on the dose, but also on the detailed distribution of the ionizing events in the tracks. Linear energy transfer (LET)[1] is a measure of this distribution, at least to a first approximation, and the need for determining the biological effects as a function of LET has long been realized. The radiations most widely used in radiobiological studies—x rays and neutrons—give broad distributions of LET in tissue and are therefore of limited value for precise LET-effects studies. Heavy ions can be produced in accelerators (Brustad et al., 1960; Hubbard et al., 1961) in almost exactly

[1] We take LET to mean charged-particle energy loss per unit path length (in keV/μ), including losses to all the secondary electrons (δ rays), regardless of their energies. This concept can be referred to as LET_{∞}. Note also that we are using the symbol μ to signify "micron," a length of 10^{-6} meter.

monoenergetic and parallel beams, which thus are suitable for quantitative studies of biological effects by the "track-segment" method (Zirkle and Tobias, 1953; Sayeg et al., 1959; Barendsen et al., 1963). The currently available beams of heavy charged particles range from protons to argon nuclei, with LET values ranging from less than 1 keV/μ to 2000 keV/μ. With the acceleration of heavier ions than Ar the LET could be extended even higher. At the time of this writing, the principles of accelerating ions of any of the elements of the periodic table to biologically useful energies have been demonstrated.

Heavy ions have been useful in cellular radiobiology. Studies with various types of unicellular organisms and with mannalian cells have already indicated that biological effects probably can be divided into three classes: those that result from a single ionizing event along a particle track, those due to cooperative action of two or more events along the track, and those that could be attributed to the "thermal-spike mechanism" at very high LET. x-Ray irradiation generally produces biological effects which can be attributed to a single ionizing event along a track, or to the cooperation of events in separate tracks. These effects depend on pH and oxygen concentration, and can be modified by chemical substances present during irradiation. They are partially reversible, in that postirradiation recovery can occur under certain circumstances. For example, in bacterial spores, heat or presence of H_2S partially reverses this type of lesion (Powers et al., 1967).

The second mechanism is responsible for the often observed increase in relative biological effectiveness (RBE) when high-LET radiation is used. There is no general agreement on the details of this mechanism; however, Lea (1955), Howard-Flanders (1958), and others have attributed it to ion clusters in the particle tracks. The increase in chromosome breaks found at high LET is explained by somewhat different reasoning by Neary et al. (1965). Further, it appears that the probability of damage, as measured by a "cross section," increases proportionally to the square of the LET, finally becoming saturated at very high LET. Except in rare instances, this effect is only slightly influenced by environmental modifiers (Manney et al., 1963; Lyman, 1965). Tobias and Todd (1964) and Powers et al. (1967) found that damage due to this mechanism cannot be reversed, as can single-event damage.

The third effect—the thermal-spike effect (Norman, 1967)—has not been very widely studied so far, largely because of the relative inaccessibility

of the very-high-LET radiations. Probably the most dramatic demonstration of such effects (although in nonbiological systems) is the production of damage tracks a few angstroms in diameter in thin sheets of dielectric matter by individual fission recoils (Fleischer et al., 1965). Such tracks can be made visible through etching, which removes the damaged material.

Heavy ions have also been very useful in molecular studies, probably because they can transfer a relatively large amount of energy to a single macromolecule (Pollard, 1953; Brustad and Fluke, 1958; Dolphin and Hutchinson, 1960; Brustad, 1961; Tobias and Manney, 1964; Henrikson, 1966). The fate of the excitation energy following such interaction is of fundamental interest, and studies of postirradiation excited states are providing new information on the nature of interactions and energy transport in macromolecules.

Perhaps the widest interest in heavy ions is due to their applicability in studies of normal and pathological states in multicellular organisms, particularly of the central nervous system, and of development and differentiation. These interests culminate in therapeutic applications which are steadily expanding (Lawrence and Tobias, 1965; Tobias and Todd, 1967). In this sense the most direct application of heavy accelerated particles is to produce controlled lesions in locations not easily accessible to surgery. Since heavy-ion beams travel along a straight line and have a fixed range, they can be optically aimed at a region within the body; their ionization properties produce deep lesions at the Bragg-peak location without undue damage to intervening or deeper tissues (Wilson, 1946).

For example, much valuable information on the location and manner of homeostatic control of body functions can be obtained by creating small lesions unilaterally or bilaterally in the hypothalamus of animals (Born et al., 1959). Other studies are aimed at understanding the organization and function of the cerebral cortex. Laminar lesions are particularly useful in this context (Malis et al., 1957; Janssen et al., 1962). It is important to produce minimal-size lesions with especially sharp boundaries. The small lesions enable one to differentiate between neighboring parts, thus obtaining information with better spatial resolution, as well as avoiding unnecessary injury. Small and sharply demarcated lesions reduce the amount of scar tissue formed, a consideration very important in medical procedures (Van Dyke and Janssen, 1963). It is likely that for treating lesions with the Bragg peak, particles with atomic numbers from 6 to 12 would be ideal.

Protons were first used on human subjects at Berkeley in 1954 (Tobias et al., 1956, 1958), when the pituitary of a patient with metastatic mammary carcinoma was irradiated. Since then therapeutic investigations have broadened continuously. At the University of Uppsala the first proton treatment of Parkinson's disease was performed (Larsson et al., 1962). A number of other medical procedures are also used (Leksell et al., 1960; Larsson et al., 1958; Larsson, 1961; Kjellberg et al., 1963, 1964; Lawrence and Tobias, 1965). Pituitary irradiation appears to be worthwhile in cases of mammary cancer, diabetes mellitus with vascular disease, malignant exophthalmos, acromegaly, and Cushing's disease. Certain types of brain tumors are also treated. Limited approaches have already been made to direct irradiation of tumor metastases, and utilization of heavy-ion beams for direct cancer therapy promises to eliminate complications due to the oxygen effect (Tobias and Todd, 1967). The oxygen effect apparently is important in x-ray therapy, since anoxic tumor cells are more resistant to x rays than are oxygenated normal cells (Gray, 1961). Both kinds of cells are equally sensitive to radiation of sufficiently high LET.

Even before the advent of space flight it became clear that protons, helium ions, and heavy ions are part of the normal radiation environment in cosmic rays and especially in the vicinity of the sun. Charged-particle fields resulting from solar flares in fact constitute a major health hazard for astronauts (Van Allen, 1961; Webber, 1963, 1966) and future colonizers of planets without a shielding atmosphere. Such flare-produced fields consist of low- and high-energy protons, and about 10% of the particles in large flares are helium ions. Heavier ions have also been detected. High-energy accelerators can be used for simulating these fields for laboratory studies.

It is expected that in a few years supersonic transport planes will carry a significant fraction of the population at altitudes of 70 000 feet or more. At these altitudes the primary biological interest is particularly in the heavy cosmic rays and the recoils produced by cosmic-ray primaries and secondaries, particularly mesons. It is known that the dose-rate levels during flight will be quite low, but the potential biological effects (especially genetic) of the heavy primaries have not yet been fully evaluated.

Negative π mesons produce nuclear stars at the ends of their tracks, and because these stars have high LET, it has been proposed that mesons might profitably be used in cancer therapy (Fowler and Perkins, 1961;

Richman et al., 1966; Raju et al., 1968). Cyclotrons and linear ion accelerators are particularly suitable for production of mesons. A meson factories for producing a high-intensity field of π^- mesons is being built at the Los Alamos Scientific Laboratory, Vancouver, Canada, and Zurich, Switzerland.

II. INTERACTION OF HEAVY CHARGED PARTICLES WITH MATTER

The absorbed dose received by an irradiated sample is a consequence of interactions of the charged particles with the sample material. These interactions are briefly reviewed here before specific dosimetry problems are considered. For more detailed discussion of these interactions, the reader is referred to Bichsel (Chapter 4, Volume I), Fano (1963), and Bethe and Ashkin (1953).

The interactions of heavy charged particles with matter can be broadly subdivided into interactions with (a) whole atoms, (b) atomic electrons, and (c) nuclei. The first two types of interactions are due to electric charge (electromagnetic or Coulomb-force interactions), and nuclear forces are also involved in (c). The type of interaction which is most probable in a given case depends on (i) the nuclear impact parameter, that is, the distance between the charged-particle trajectory and the nucleus, in the absence of an interaction (Rossi, 1952); (ii) the kinetic energy of the particle; and (iii) the nature of the bombarding particle and of the atom or nucleus involved in the collisions.

(i) When the nuclear impact parameter is much larger than the atomic dimensions, the charged particle interacts with the atom as a whole, displacing it from its normal position.

(ii) When the nuclear impact parameter is comparable to atomic dimensions, the interaction is mainly between the charged particle and the atomic electrons. If the energy acquired by the electron is large compared with its binding energy, this process can be treated as an interaction between the charged particle and a free electron. If the resulting secondary electrons are energetic enough, they can cause further ionization of atoms, and are called δ rays.

(iii) When the nuclear impact parameter becomes smaller than the atomic radius, in addition to interacting with electrons, the incoming charged particle is deflected owing to the Coulomb field of the nucleus. For nuclear impact parameters smaller than nuclear radii, nuclear reactions can take place if the kinetic energy is high enough.

Thus, as a result of electromagnetic interactions, heavy charged particles lose energy by ionization and excitation of atoms in the absorbing medium. Successive small deflections due to Coulomb interactions between the charged particle and the nuclei of the medium (multiple scattering) cause the particle beam to spread transversely as it passes through the medium. Elastic collisions with atoms play an insignificant role in the energy loss of heavy charged particles, except at very low energies. The energy at which elastic collisions with atoms become more important than the electron collisions in the energy-loss process varies with the type of heavy charged particle under consideration (Lindhard, 1964; Snyder and Neufeld, 1957); for example, this energy is approximately 1.5 keV for protons, 94 keV for carbon ions, and 180 keV for oxygen ions. It has been shown by Jung (1967) that the radiobiological effect is very significant for protons of energies less than 1 keV. This result confirms the importance of elastic collisions with atoms at such low energies.

Inelastic collisions with nuclei, that is, those in which nuclear reactions occur, depend primarily on the type and energy of the heavy charged particle and on the nature of the nuclei in the medium. The penetration of secondary particles produced in these reactions must be considered separately. Table I shows the probabilities of protons' penetrating different thicknesses of carbon and lead absorbers without undergoing nuclear interactions (see also Janni, 1966). The primary beam intensity decreases exponentially with increasing absorber thickness when nuclear interactions are the controlling process.

A. Energy Loss

Heavy charged particles, as they pass through matter, lose energy chiefly through interactions with atomic electrons. This process leads to a gradual decrease of energy as the particles pass through the stopping medium. For example, the residual energy of a 10.4 ± 0.05 MeV/amu* ^{28}Si heavy-ion beam as it passes through aluminum is shown in Fig. 1. The rate of energy loss is proportional to the square of the charge of the incident heavy particle, and approximately inversely proportional to its kinetic energy. As the particle proceeds through the medium, it slows down gradually; and its rate of energy loss therefore increases. At very low velocities the particle captures electrons,

*amu is the number of atomic mass units; the initial kinetic energy of this silicon beam is 291.2 MeV.

Table I. Probability of proton nuclear interactions as a function of absorber thickness.[a]

Proton energy (MeV)	Shielding thickness (g/cm^2)	Residual energy (MeV)		Fraction of protons not undergoing nuclear interactions in the shielding	
		Carbon	Lead	Carbon	Lead
100	5	61	81	0.95	0.98
150	5	123	135	0.95	0.98
	10	92	121	0.90	0.95
300	5	285	290	0.95	0.98
	10	265	280	0.91	0.96
	50	87	200	0.61	0.80
600	5	590	590	0.95	0.97
	10	575	580	0.90	0.95
	50	480	530	0.58	0.77
	100	340	455	0.33	0.59
	150	162	385	0.19	0.46
1000	5	990	990	0.95	0.98
	10	980	980	0.90	0.95
	50	900	940	0.60	0.79
	100	800	880	0.34	0.62
	150	685	820	0.20	0.49
	200	570	760	0.12	0.38

[a]Bobkov et al. (1964).

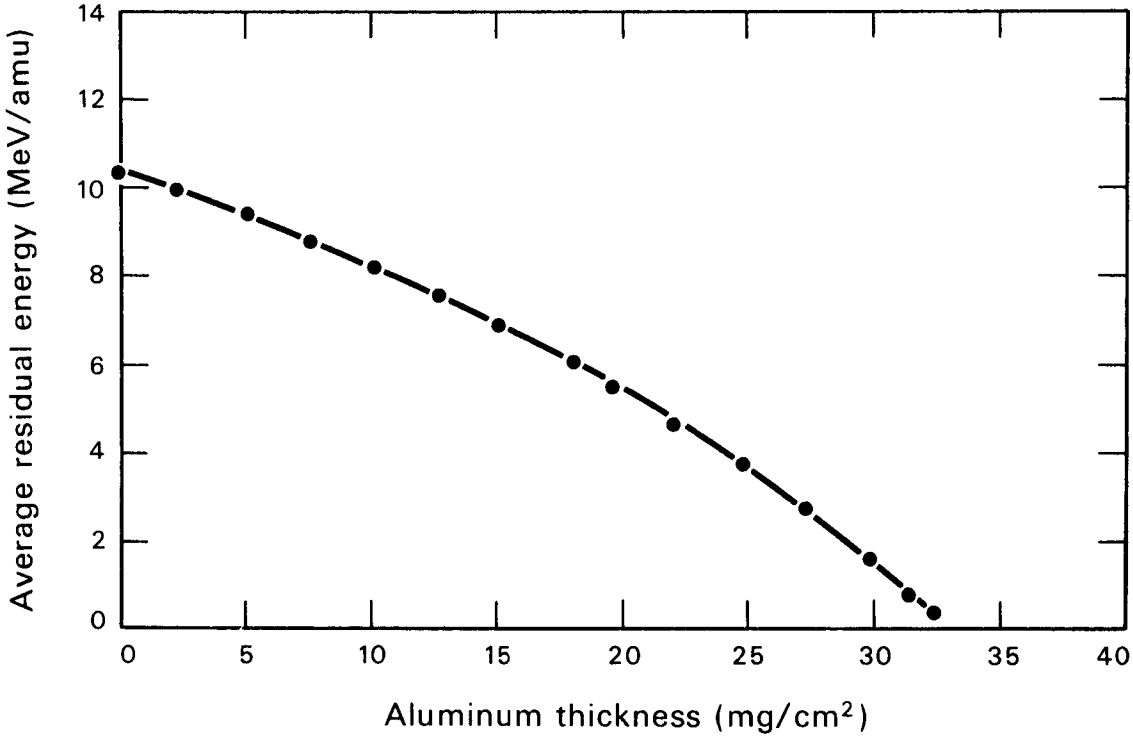

DBL 6712-1905

Fig. 1. Average residual energy of a ^{28}Si heavy-ion beam of initial energy 10.4 MeV/amu as a function of thickness of aluminum penetrated. It can be seen that the energy near the end of the path decreases much more rapidly than at the beginning.

as a result of which the effective charge of the particles is reduced. Consequently the rate of energy loss per unit track length decreases at very low velocities. The heavy charged particle continues to slow down until its energy is reduced to the thermal energy of the atoms in the medium.

The deceleration process occurring while heavy charged particles are completely ionized can be adequately treated by stopping-power theory. However, when the particles slow down enough to capture electrons (below 2 MeV for helium ions or 0.4 MeV for protons), the theoretical problems become difficult, and the effect of such capture upon the range of the particles must be obtained from experimental data. The average rate of energy loss (in MeV per g/cm^2, i.e., mass stopping power) for a nonrelativistic heavy charged particle of velocity $v = \beta c$ (cm/sec) traversing an infinitesimal segment of path length is given by

$$S = \frac{0.307}{\beta^2} \frac{z^2}{A} \cdot B , \qquad (1)$$

where B is equal to $Z[\log 2mc^2\beta^2 - \log(1 - \beta^2) - \beta^2 - \log I] - C$, c is the velocity of light, z is the charge number of the incident particle, A is the atomic weight of the medium, B is the stopping number, Z is the nuclear charge of the absorber, I is the average excitation potential of the medium, and C is the sum of the shell corrections (Walske, 1952, 1956). For practical calculations of proton stopping power see Chapter 4, Section II, C and H (Volume I). The stopping powers of water and lead for protons over a wide range of energies are shown in Fig. 2.

The stopping-power formula, Eq. (1), can be used for low-energy ions if the effective charge z_f^* is used in place of z. For the heavy ions ^{12}C and ^{40}Ar, for example, the maximum specific ionization (or stopping power) occurs at energies of approximately 8 and 65 MeV, respectively (Northcliffe, 1964). At lower energies the decrease of z_f^* overcompensates the increase in energy loss resulting from the influence of the β^2 term in Eq. (1). This effect is the same as that which occurs for protons at much lower energies.

Tables of stopping powers for various elements and types of heavy charged particles are given in Chapter 4 (Volume I) and by Barkas and Berger (1964), Trower (1966), Williamson et al. (1966), Janni (1966), and Bichsel (1963).

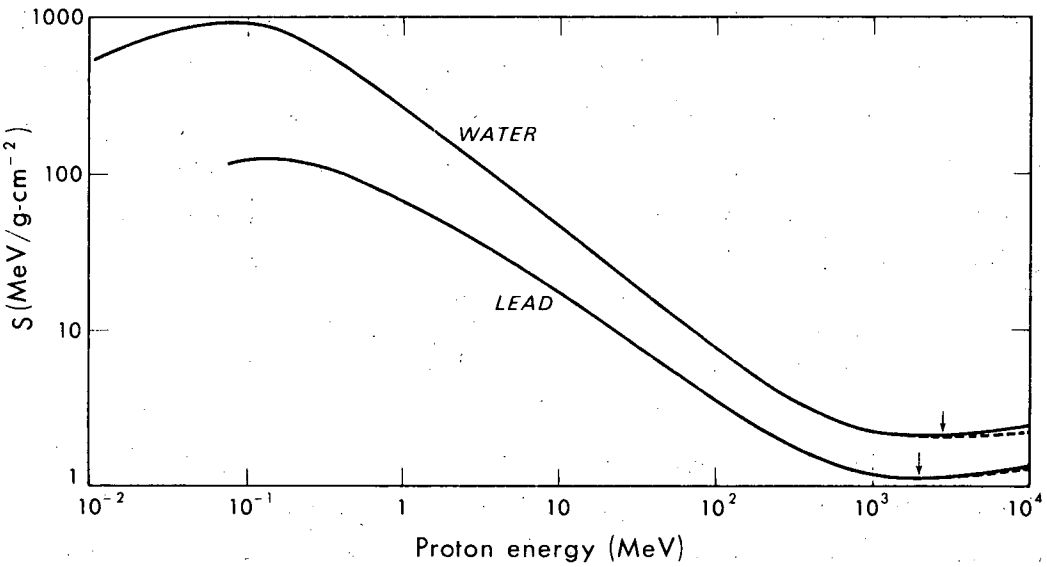

DBL 675-1626

Fig. 2. Stopping power of protons of energies from 20 keV to 10 GeV, in water and lead (data taken from Whaling, 1958; Barkas and Berger, 1964). Arrows indicate the energy at which the stopping power is minimum. Dashed lines indicate values after density-effect correction for water. At energies below 80 keV, the stopping power decreases with decreasing energy. This is partly due to the reduction of effective charge. At intermediate kinetic energies, from 100 keV up to about 1 GeV, the energy region of interest for biomedical studies, the stopping power decreases with increasing energy, reaching a minimum near an energy equal to around twice m_pC^2, the rest energy of the charged particle. At still higher energies, where the velocity of a proton approaches that of light, the term $-\log(1-\beta^2)$ in the stopping number B will cause the stopping power to increase with particle energy. A further correction is necessary for condensed materials. It is known as the density-effect correction and causes a reduction of stopping power. It is discussed extensively by Sternheimer (1966).

It follows from Eq. (1) that the ratio of the stopping power for a particle with charge number z_1 to that of another particle with charge number z_2 is given to a first approximation by

$$\frac{S_1}{S_2} = \frac{z_1^2}{z_2^2} \tag{2}$$

when the particles travel with equal velocity through the same material. Hence from stopping-power tabulations for protons, one can calculate the stopping power of any other heavy charged particle of like velocity from Eq. (2). In general, where the two velocities differ, one first finds the energy E of a proton (mass M) which has the same velocity as that of the other particle having mass M_1 and energy T_1, thus: $E = T_1(M/M_1)$. The proton stopping power (S_2) at energy E is then obtained from tables, and Eq. (2) is applied to compute S_1. Examples of this procedure and all the necessary tables will be found in Chapter 4 (Volume I) (see Section IIC).

The stopping powers of two substances with atomic masses A_a and A_b for a particle with a given velocity may be compared, independently of the densities of the substances,* by considering the relative mass stopping power S_m,

$$S_m = \frac{S_a}{S_b} = \frac{A_b}{A_a} \cdot \frac{B_a}{B_b}, \tag{3}$$

where the symbols are defined as in Eq. (1), and the subscripts a and b refer to the two materials.

In obtaining the stopping power of a compound, we assume that the contributions from the individual atoms that comprise the compound are additive (Bragg's rule). This method neglects any effects of the electronic binding in molecular compounds. Slight deviations from the additivity rule exist, but these are generally not significant in radiobiology. Thus we can calculate the heavy-particle stopping power of compounds from the data given for the various elements in tables such as those of Barkas and Berger (1964). It is important to note that the stopping-power values derived in this way apply to compounds

*Except that the value of I must be appropriate to the state (gaseous or condensed) of each medium (e.g., see Sternheimer, 1966).

which, at a macroscopic level, are homogeneous and isotropic. This raises a conceptual problem in their evaluation in radiobiology at the submicroscopic level, since living cells are anisotropic and inhomogeneous in their chemical composition. Usually, one also ignores variations in the density of subcellular particles. Engstrom and Lindstrom (1958) have shown, however, by the method of quantitative x-ray microscopy, that in certain cells the density of the nucleus may be twice that of the cytoplasm. The density of DNA preparations separated from living cells by homogenizing the cells and centrifuging in a density gradient is between 1.5 and 1.7 g/cm^3.

B. Range-Energy Relation

Below energies at which nuclear collisions are important, a monoenergetic beam of heavy charged particles traversing matter will gradually lose energy to electrons by ionization and excitation, while the total number of primary particles in the beam remains essentially unchanged. The particles will finally be stopped after they have traveled approximately equal path lengths in the absorber. The interactions with electrons are subject to statistical fluctuations, hence there will be fluctuations in the path lengths of individual particles (called range straggling) amounting to about 1% of the mean path length, or range, R (Wilson, 1946). Energy-loss fluctuations are discussed in Section IV.

The thickness of material which will be penetrated by a perpendicularly incident monoenergetic beam of particles can be specified in several ways, as discussed in Chapter 4, Section III, A (Volume I). One useful concept is that of extrapolated range R_p, which is defined as the absorber thickness occurring at the x-axis intercept of the tangent drawn through the point of the curve's steepest descent, as illustrated in Fig. 3. Because relatively few heavy particles are observed to penetrate beyond this thickness, its value evidently approaches that of the maximum path length. Another concept often employed is the median projected range, t_{median}, also shown in Fig. 3. This is the absorber thickness traversed by half the incident particles, assuming that none are lost prematurely in catastrophic events such as nuclear reactions or bremsstrahlung production. The idealized curve in Fig. 3 has zero slope, indicating the absence of such catastrophic events, for absorber thicknesses less than that at which the final rapid decrease occurs. Actually t_{median} has to be defined as the thickness at which the number of particles is one half of the number of incident particles reduced by the number of particles removed

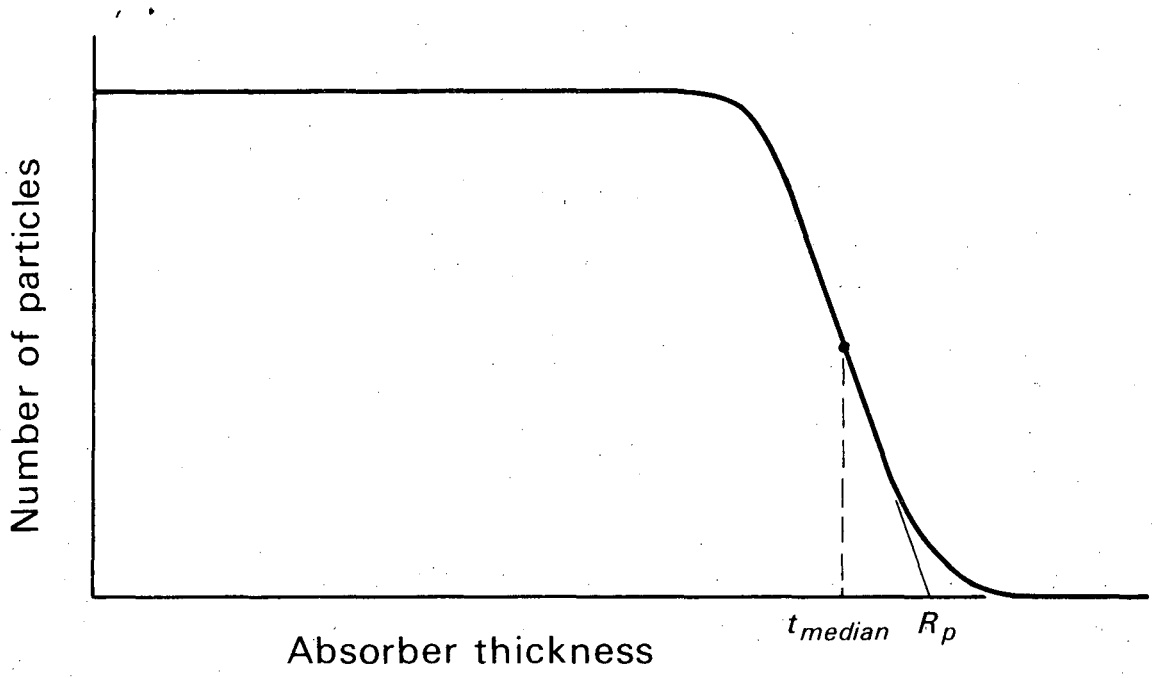

DBL 675-1627

Fig. 3. Number-distance curve showing the number of particles in a beam penetrating to a given depth. The median projected range is indicated as t_{median} and the extrapolated range as R_p.

from the beam by nuclear reactions. If the slope is not zero to the left of the knee (e.g., Fig. 19), t_{median} is based on halving the number of particles reaching the latter depth. The term t_{median} has approximately the same value as the projected range $\langle t \rangle$ (defined in Chapter 4), which in turn approximates the mean path length R for heavy particles because they are not readily scattered and thus tend to follow straight paths.

The difference between the R_p and t_{median} is related to the straggling parameter (Hubbard and MacKenzie, 1952). For a given range, straggling is less for heavier particles. For a given particle, straggling increases with the particle energy, because of the increasing importance of nuclear interactions.

From Eq. (1) the average path length segment $(\Delta R)_{z,M}$ traversed in an absorber by completely ionized heavy particles of mass M and atomic number z, for a decrease in kinetic energy from T_1 to T_2, is

$$(\Delta R)_{z,M}(T_1 - T_2) = \int_{T_2}^{T_1} (1/S)dT \, . \qquad (4)$$

In principle, the range R of particles of initial energy T_0 is obtained by integrating Eq. (4) from T_0 to zero energy. The ranges of two different types of particles passing through the same stopping material with equal initial velocities V_0 are related by

$$R_1(v_0) \approx \frac{M_1}{M_2} \frac{z_2^2}{z_1^2} R_2(v_0) \, . \qquad (5)$$

Equation (5) can be employed to compute the approximate range of other particles from the tabulated values for protons, remembering that the energies of particles having the same velocity are inversely proportional to their masses. The capture of electrons by heavy charged particles, especially when they are multiply charged and of low velocity, tends to extend their range. Equation (5) can be corrected for this by use of effective z values, as discussed in Chapter 4, Section II G, or through the formulas provided by Barkas and Berger (1964) (formulas 6-11).

Theoretical range-energy and stopping-power relationships among various heavy ions in water are given in Fig. 4 (Steward, 1967). Several recent theoretical range-energy tables are available (Chapter 4, Volume I;

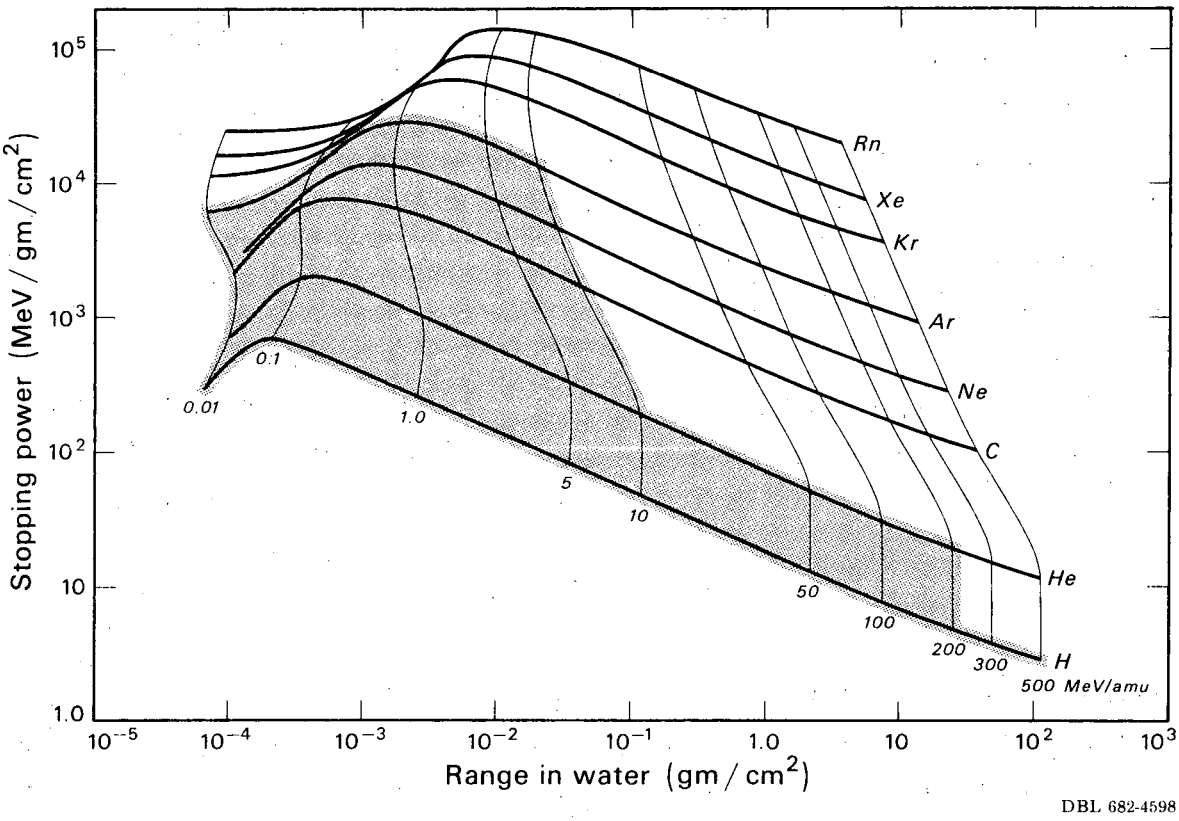

Fig. 4. Theoretical range energy and stopping power for various heavy ions in water (Steward, 1967). Shaded area indicates the energies of the currently available heavy charged particle beams.

Barkas and Berger, 1964; Williamson et al., 1966; Janni, 1966). A computer program for the calculation of the energy loss of heavy charged particles is given by Bichsel (1967).

C. Multiple Scattering of Heavy-Charged-Particle Beams

When a parallel beam of heavy charged particles passes through a medium, the particles are scattered and the beam diameter is gradually expanded with increasing depth, mainly due to Coulomb-force interactions between the incident particles and the nuclei of the medium. This scattering is due partly to the cumulative effect of many small deflections, and partly to large single-event deflections of relatively few of the particles. The first type of process is called multiple scattering, while the second is referred to as single scattering. For most practical applications multiple scattering through small angles, represented approximately by a Gaussian distribution, predominates over single scattering. The mean square angle of multiple scattering when the absorber thickness is small is given approximately by

$$\langle \theta^2 \rangle = \left(\frac{21}{\beta c p} \right)^2 \frac{x}{\ell} z^2 , \tag{6}$$

where θ is in radians, p is the particle momentum in MeV/c, z is the charge of the particle, x is the absorber thickness, and ℓ is the radiation length in the absorber (see Rossi, 1952). The root-mean-square scattering angle is evidently proportional to the charge of the incident particle and the atomic number of the medium, and (in the nonrelativistic case) inversely proportional to the kinetic energy of the particle.

The variance of the Gaussian distribution, which represents the effect of multiple scattering at a distance X_0 from the exit surface of the absorber for a particle beam having an initial range R_0 and residual range R, is given by

$$\sigma^2 = \int_R^{R_0} \bar{\alpha}^2 (R' - R + X_0)^2 dR' , \tag{7}$$

where

$$\bar{\alpha}^2 = \lim_{x \to 0} \langle \theta^2 \rangle / x .$$

If one is interested in finding the width of the Gaussian distribution inside the absorber, then X_0 in the above expression is zero. It can be seen that the width of the

Gaussian distribution representing the multiple scattering increases with the increase in X_0, even if the thickness of the scattering medium remains the same.

Starting from Williams' theory of multiple scattering and making some reasonable assumptions, Preston and Koehler (1968) obtained the following empirical expressions for the standard deviation σ_0 in centimeters at the end of the range R_0(cm) for a proton beam of originally negligible diameter:

$$\sigma_0 = 0.0307\, R_0 \quad \text{(protons in water)}, \tag{8}$$

$$\sigma_0 = 0.045\, R_0 \quad \text{(protons in aluminum)}. \tag{9}$$

Figure 5 gives the standard deviation σ at any fraction of the proton range in terms of the standard deviation σ_0 at the end of the range. It can be seen from Fig. 5 that the Gaussian width due to multiple scattering increases rapidly near the end of the range. If the incident beam profile is close to a Gaussian distribution of width σ_i in the absence of the scattering material, then the standard deviation due to scattering in the medium can be obtained from the measured standard deviation σ_m by using the expression

$$\sigma^2 = \sigma_m^2 - \sigma_i^2 . \tag{10}$$

Figure 6 shows the changes in the beam profiles due to multiple scattering (calculated) of a helium-ion beam at different fractions of the residual range (Sperinde, 1967). It can be seen from Fig. 6(A) that for a small collimated beam (2-mm diameter), the intensity at the central axis of the beam becomes smaller as the beam passes through the medium. Hence the full width at half-maximum of the beam is increased considerably near the end of the range. On the other hand, for large collimated beams (such as 20-mm diameter) it can be seen from Fig. 6(B) that the full width at half-maximum, as well as the intensity on the central axis, remains essentially the same although the edges of the beams are rounded off. This must be taken into consideration when narrow beams are used for making lesions for some biological applications.

A useful relation for proton and helium-ion beams of the same range is that the multiple scattering of a helium-ion beam is half that of a proton beam. Multiple-scattering calculations for protons have been given by Janni (1966).

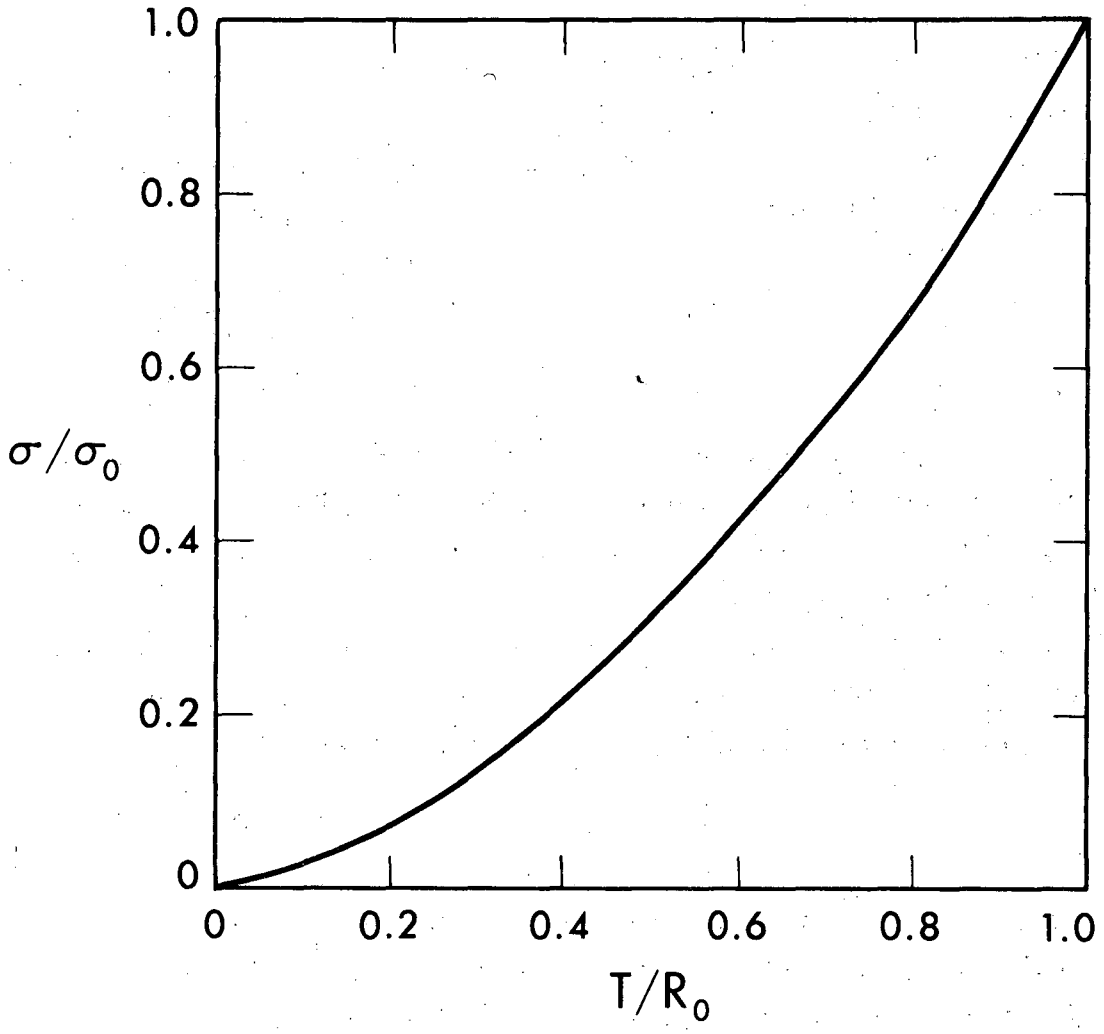

DBL 675-1628

Fig. 5. The calculated ratio of the standard deviation for protons, at depth T in a given material, relative to that at the end of the range R_0 (Preston and Koehler, 1968).

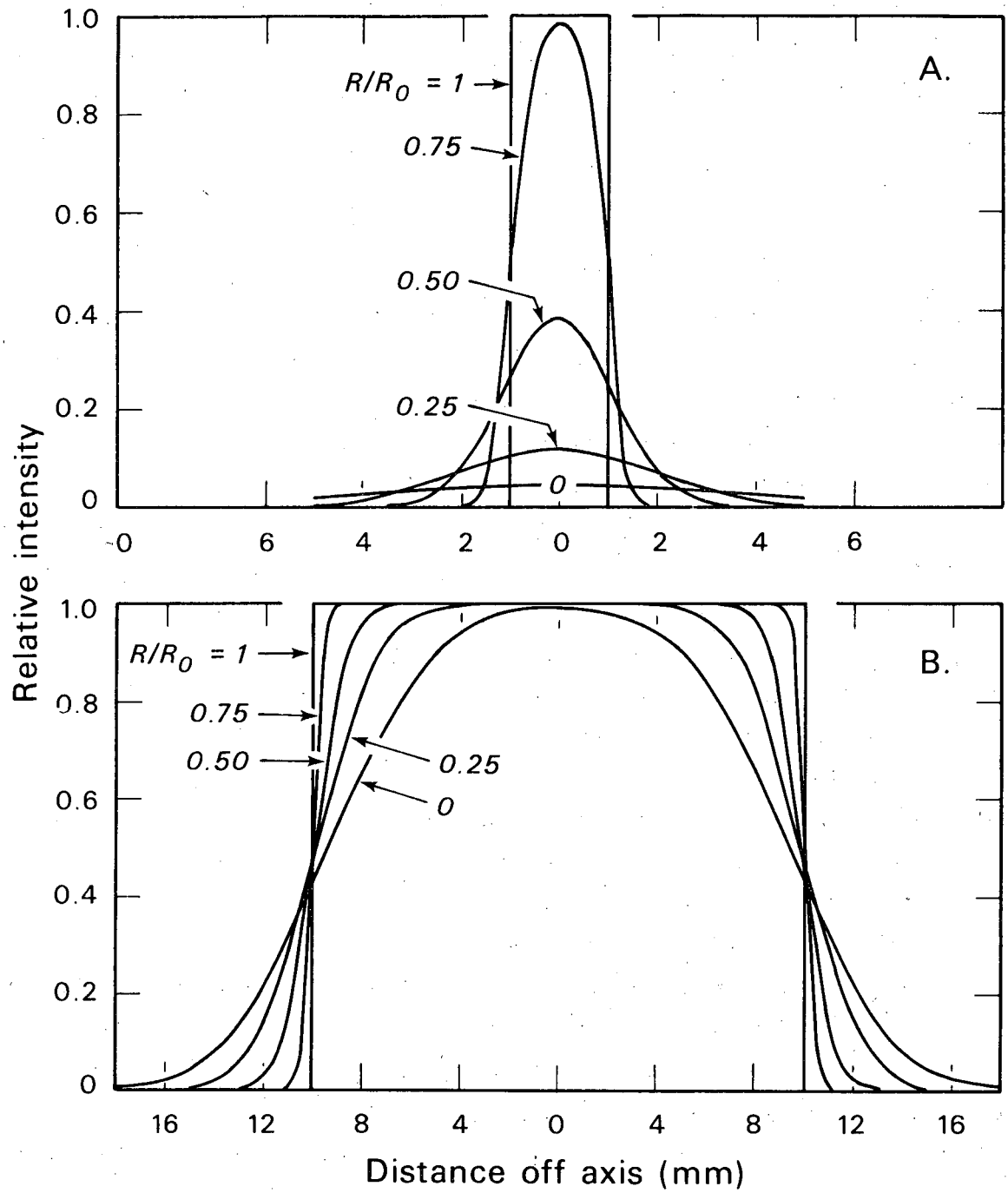

DBL 675-1629

Fig. 6. Relative intensity (particles) of the beam as a function of distance off the central axis. The terms R_0 and R are the range and residual range, respectively. Absorption is neglected; the change is due to scattering alone (Sperinde, 1967). (A) 2-mm-diameter beam; (B) 20-mm-diameter beam.

Preston and Koehler (1968) also calculated the intensity of the beam along the axis as a function of depth in the medium for both circular and rectangular apertures. The intensity $I(x, 0, 0)$ on the axis at a depth x for a uniform circular beam of radius r_c is given roughly by the expression

$$I(x,0,0) = \frac{1}{\pi\sigma_x^2} \int_0^{r_c} 2\pi r \exp[-r^2/\sigma_x^2]\, dr = 1 - \exp[-r_c^2/\sigma_x^2]. \quad (11)$$

For a uniform beam of 128-MeV protons of total range $R_0 = 12$ cm of water, the plots for Eq. (11) are shown in Fig. 7 for various beam sizes. It can be seen from the figure that, with a decrease in beam size, the number of particles per unit area along the axis decreases considerably as a function of depth of penetration. The loss of particles due to nuclear interactions is neglected in the above calculations; the number of protons in the beam actually decreases to some extent with penetration into the medium as a result of nuclear interactions (see Table I and Fig. 19). At the same time, the proton stopping power increases with depth as the velocity decreases, until a maximum is reached (at the Bragg peak) near the end of the range. Hence the dose delivered by a heavy-charged-particle beam varies as a result of all these factors: scattering, nuclear interactions, and change of stopping power. The relative doses on the axis of a monoenergetic proton beam for beams of different radii, as calculated by Preston and Koehler, are shown in Fig. 8, where it can be seen that the effect of scattering is negligible for a beam of sufficiently large radius, r_c, that is, for $r_c >> \sigma$. For such large beams the dose deposition on the beam axis depends only on absorption of particles by nuclear reactions and on change of the stopping power. On the other hand, for small collimated beams the effect of multiple Coulomb scattering becomes important, and the central axis dose at depth becomes smaller owing to particles' scattering out. The experimental results agree fairly well with the above-mentioned approximate calculations of multiple scattering of heavy-charged-particle beams. Some experimental data are given in Section IV.

For a given range, the Gaussian width due to multiple scattering becomes smaller as the atomic number of the heavy ions increases. Heavy ions, then, may prove to be more useful than other particles when narrow beams are needed for radiological cutting purposes (Litton et al., 1967).

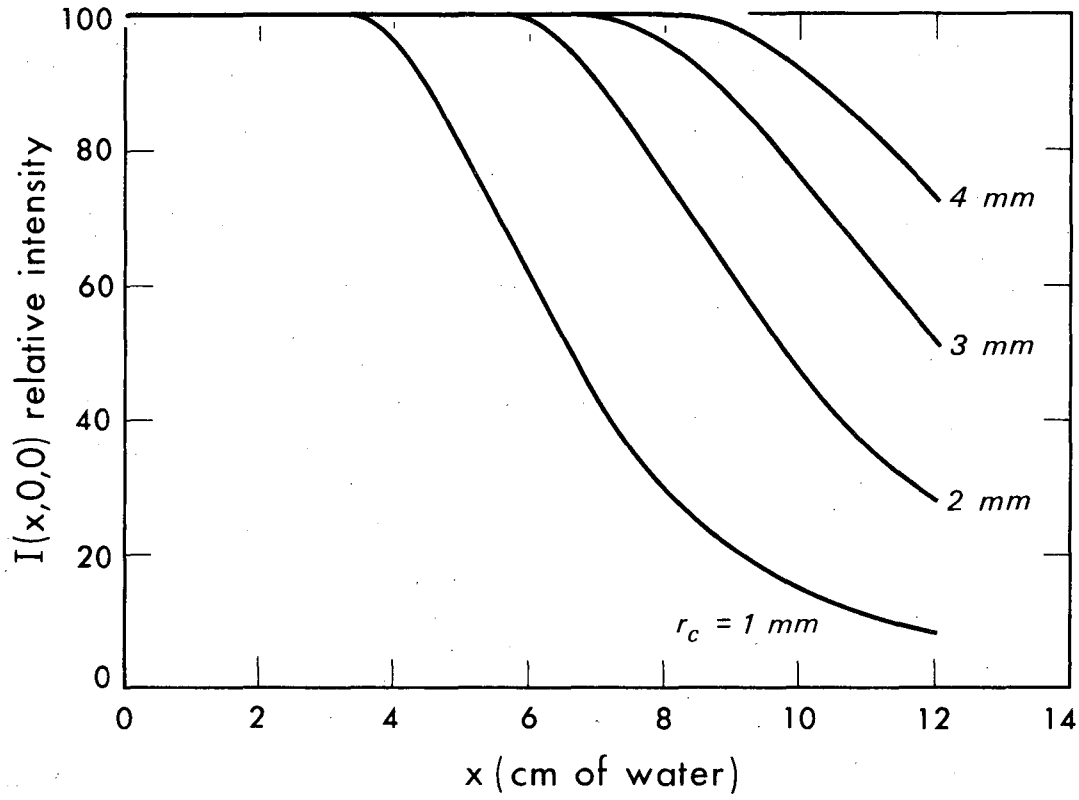

DBL 675-1630

Fig. 7. Calculated relative intensity (particles), I(x, 0, 0), on the axis of a uniform circular beam of initial range R_0 = 12 cm of water and radius r_c at the collimator, as a function of depth x in water. Absorption is neglected; the change is due to scattering alone (Preston and Koehler, 1968).

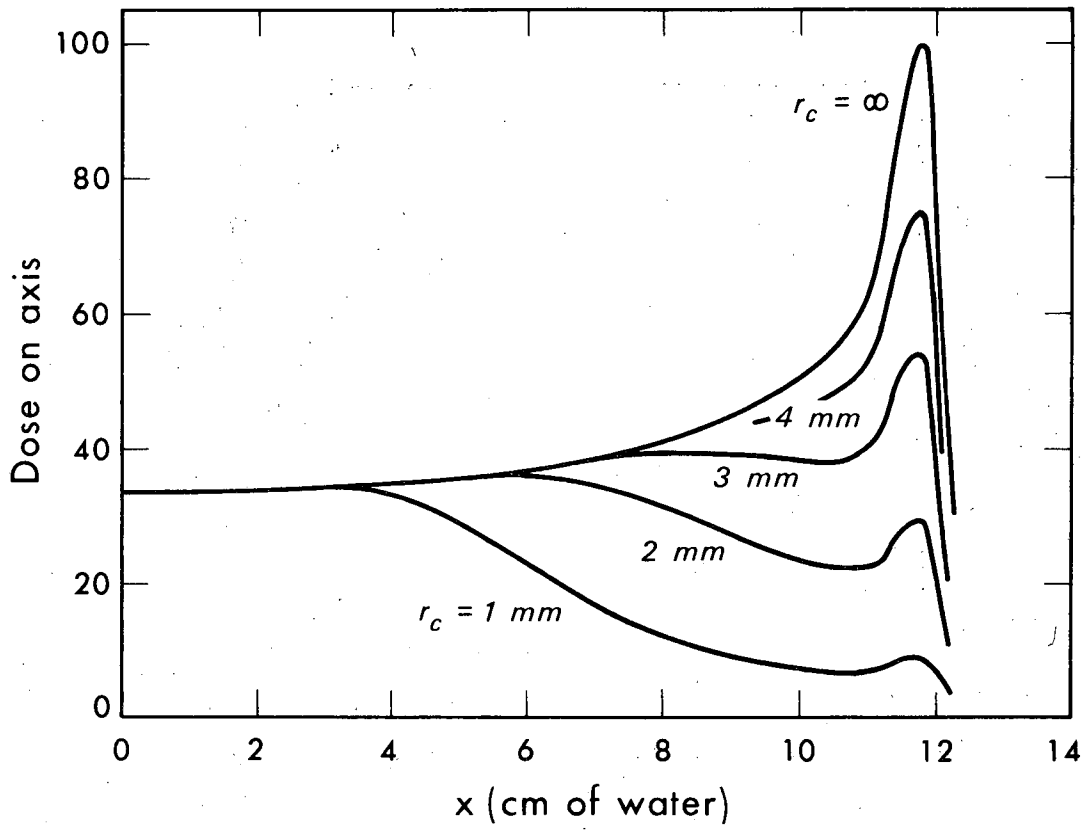

DBL 675-1631

Fig. 8. Relative dose on the axis of a uniform circular proton beam, of initial range R_0 = 12 cm of water and radius r_c at the collimator, as a function of depth x in water. The curve $r_c = \infty$ is an experimental Bragg curve; the others are calculated (Preston and Koehler, 1968).

III. DETECTORS OF HEAVY CHARGED PARTICLES

Many different types of detectors have been used to measure and monitor heavy-charged-particle beams. We limit our discussion to ionization chambers, Faraday cups, secondary-emission monitors, and activation dosimeters, which are the most extensively used, and semiconductor detectors, which offer a relatively new and very useful method for energy and energy-loss measurements. By limiting our discussion to these detectors, we do not imply that other detectors are not useful also in some cases for measuring heavy-charged-particle beams. Proportional counters, scintillation detectors, chemical dosimeters, solid state integrating dosimeters, photographic emulsions, and calorimeters are all applicable in this connection, and have been described in the appropriate chapters of Volume II.

A. Ionization Chamber

The instrument most often used to measure dose delivered by heavy charged particles is the parallel-plate ionization chamber. (A general treatment of ionization chambers is in Chapter 9, Volume II.) Two types of such chambers are shown in Fig. 9. The collection volume for such a chamber can be limited to the central part of the beam by making the collection electrode small. This can be done, for example, by making a circular "scratch" through an evaporated aluminum coating on a Mylar substrate. Electrical connection to this collection electrode is made from the back side of the electrode with a fine wire or an electrically conducting film (i.e., Aquadag, evaporated Al coating, or conducting silver paint). When a sufficiently large guard-ring electrode surrounds the collection electrode, the electric field may be assumed to be uniform and parallel. The collection volume, which must be known for the dose calculation, is then defined by the area of the collection electrode and the distance between the high-voltage and collection electrodes. The electrodes may be made of thin metal foil, or Mylar foil coated with an electrically conducting film.

Since heavy-particle beams from accelerators fluctuate in intensity, the current from the ionization chamber is usually integrated by charging a capacitor and measuring the potential thus developed across it with the aid of an electrometer. It is advantageous to use an electrometer with nearly 100% inverse feedback so that the collection electrode is always held effectively at ground potential. This reduces (a) the collection of stray ions from regions of the chamber outside the intended sensitive volume, (b) the leakage of

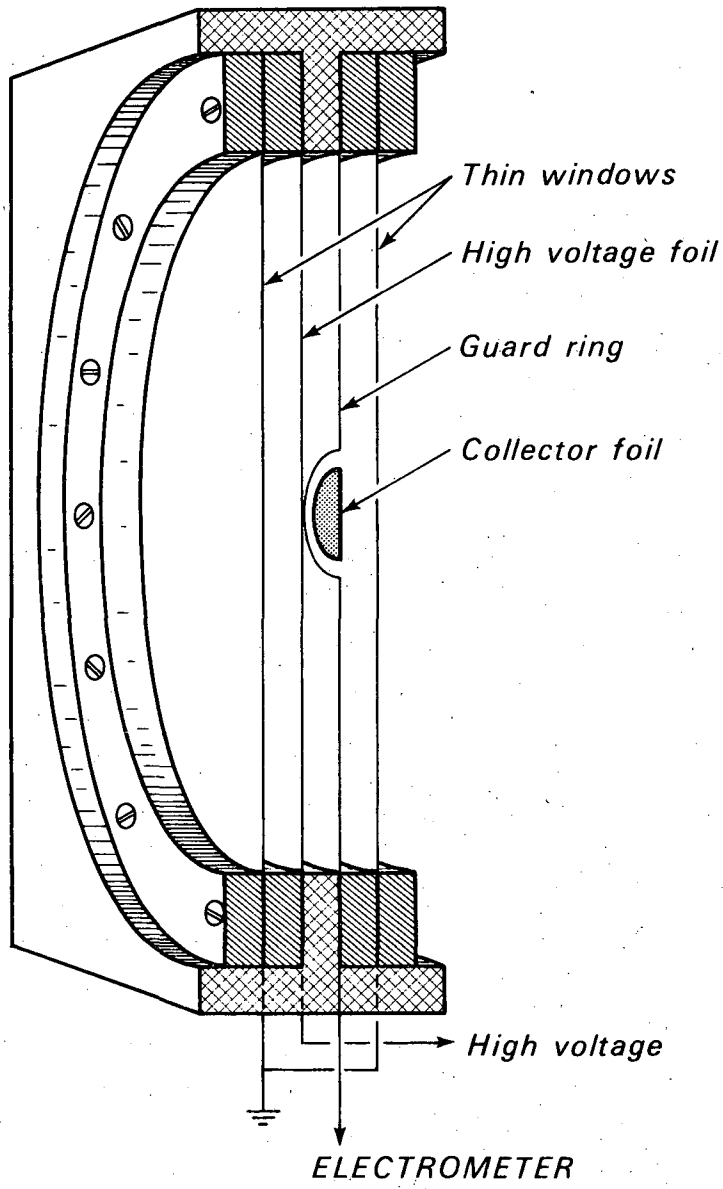

DBL 676-1675

Fig. 9. Perspective view of large-area and limited-area ionization chambers.

charge from the collector to ground, and (c) the response time of the electrometer circuit.

The Bragg-Gray principle as it applies to dose measurement was treated extensively in Chapter 8 (Volume I). For heavy charged particles, however, the primary interactions that result in ionization of the gas occur principally in the gas (rather than in the wall of the chamber, as for γ radiation); hence the atomic composition of the wall is not critical. For example, it has been shown experimentally that the effect of aluminum foils is not significantly different from that of low-atomic-number materials like Mylar (Welch, 1967).

If the charge Q (coulombs) is collected from an ionization chamber, the dose D (rads) in a target located at the same position is

$$D = \frac{10^5 Q W S_m}{\rho V} \tag{12}$$

Here V is the collection volume of the ionization chamber (cm^3), ρ is the density (g/cm^3) of the ionization-chamber gas at ambient temperature and pressure, W is the energy per ion pair (eV) for the gas, and S_m is the ratio of the mass stopping power of the target material to that of the gas, for the heavy particles present. The factor 10^5 comes from the conversion of the units of measurement, that is, charge per ion pair to coulombs, and electron volts per gram to rads.

In many applications the dose must be measured by an ionization chamber located away from the target: for example, when the target is an organ deep within the body and the ionization chamber is at the surface. The dose received by the target differs from the dose measured at the surface because of divergence of the beam, scattering by intervening material, and the Bragg depth-dose effect. Then the dose D_A delivered to the target at point A can be calculated from the charge Q collected from an ionization chamber located at point B near the surface of the subject, by the relation

$$D_A = \frac{10^5 Q W (S_m)_A K}{\rho V} \quad . \tag{13}$$

Here $(S_m)_A$ is the ratio of the mass stopping power of the target material to that of the ionization-chamber gas for particles with the energy of those at point A. Values of $(S_m)_A$ can be calculated from tabulated stopping-power

data (Barkas and Berger, 1964). The average energy of the particles at point A can be determined by subtracting from their initial energy (at B) the amount of energy lost in passing through the absorber to A, by means of the range-energy relations (Barkas and Berger, 1964). K is the ratio of the energy loss per gram of gas in an ionization chamber at position A to that in the ionization chamber at position B.

The factor K can be determined experimentally by constructing a tissue-equivalent phantom to represent the subject, and measuring the charge collected in two ionization chambers located at points A and B, as above. Then K is obtained from the relation

$$K = \frac{Q_A W_A V_B \rho_B}{Q_B W_B V_A \rho_A} , \qquad (14)$$

where the subscripts refer to the ionization chambers located at points A and B, and ρ_A and ρ_B are the densities of the gases in the ionization chambers at points A and B. The values of W for different gases are discussed in Chapter 7 (Volume I). An additional correction to the dose measurement for any nonuniform intensity distribution of the beam may be required (Birge and Sayeg, 1959).

In the design of chambers, pulse characteristics of the beams must be considered, and the collection voltage must be high enough to ensure full ion collection (Chapter 9, Volume II; Santoro and Peele, 1964) or at least to make the necessary corrections for recombination of ions acceptably small.

B. Faraday Cup

The Faraday cup (Chamberlain et al., 1951; Palmieri and Goloskie, 1964; Santoro and Peele, 1964) is often used as a primary standard to determine the number of particles in a charged-particle beam. The charge-collection efficiency of a well-designed cup is independent of the beam intensity. The Faraday cup consists of an absorber block, thick enough to stop all the primary beam and its secondary charged particles. This block, generally cup shaped, is supported by insulators within an evacuated chamber. Care must be taken in designing the Faraday cup so that the net charge collected is only that delivered by the beam.

A Faraday cup in use at the 184-inch synchrocyclotron at Berkeley for energetic charged-particle beams with ranges less than about 100 g/cm^2 of copper is shown in Fig. 10. The following factors are to be considered

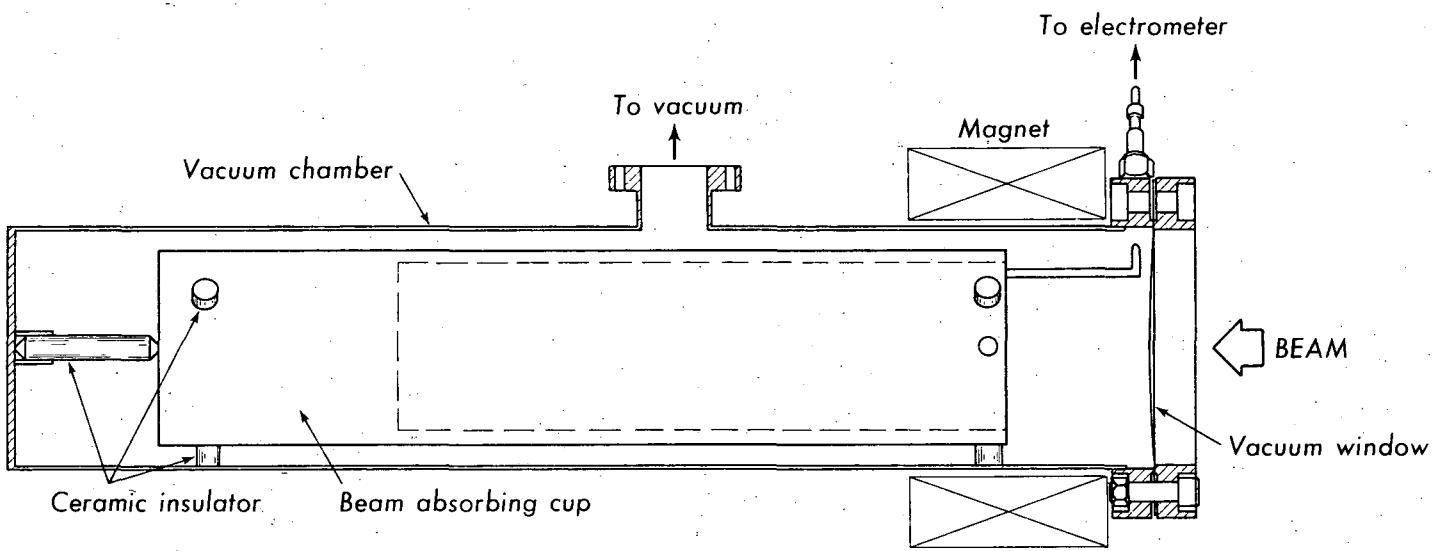

Fig. 10. Cross-sectional view of a cylindrical Faraday cup. The absorber block referred to in the text is labeled "beam absorbing cup."

in the selection of the material for the Faraday cup. The mean free path in the material should be long enough to minimize the nuclear secondaries. The density of the material should be high, to minimize the linear range and the beam spread. The material should have a low coefficient for the emission of secondary electrons in order to minimize the escape of secondary electrons from the surface. Copper is a practical compromise. The inner radius of the cup should be large enough so that the primary beam does not strike the cup wall.

The outer radius of the Faraday cup should be greater than the beam radius by at least three times the mean radial beam spreading. For energetic primary beams, in which there is fairly high probability of the particles' having an inelastic nuclear collision followed by emission of energetic secondary particles, the radius of the cup must be even larger, since the secondary particles have a greater angular spread than the primary beam. The radius of the Faraday cup for such a beam can be determined by means of the blackening of photographic film. The cup should be deep enough so that the solid angle through which back-scattered secondary electrons may escape is acceptably small.

Most of the secondary electrons that escape from the surface of the cup have energy less than 50 eV, therefore the wall thickness is not an important factor in containing the secondary electrons. Secondary electrons should be prevented from entering or leaving the collection block. A magnetic field of approximately 1000 gauss, oriented perpendicular to the axis of the beam, is sufficient to cause low-energy secondary electrons to return to the surfaces from which they are emitted. Detailed calculations of secondary-electron trajectories in the magnetic field of a Faraday cup are reported by Pruitt (1966). If an ion pump or an ionization gauge is used in connection with the vacuum system of the Faraday cup, spurious leakage currents may be caused; it is advisable to shut these auxiliary instruments off whenever measurements are made.

The number of particles N stopped in a Faraday cup is given by the relation

$$N = \frac{Q_F}{ze} \quad , \tag{15}$$

where Q_F is the charge (in coulombs) collected, z is the average number of charges carried per particle, and e is the electronic charge in coulombs.

Under these conditions, the total energy (E) transferred (in MeV) is

$$E = NT, \tag{16}$$

where T is the kinetic energy (in MeV) of the particle entering the cup.

Often the quantity of interest is the number of particles incident per unit area, called the particle fluence Φ (ICRU, 1962),

$$\Phi = \frac{\Delta N}{\Delta a} . \tag{17}$$

To determine the fluence through a small area from the total number of particles in the beam, it is necessary to know the profile of the beam, since it may not be of uniform intensity over its entire area a. Knowing the particle fluence (particles/cm^2) in the target material, one can calculate the dose D in rads from

$$D = 1.602\Phi\left(-\frac{1}{\rho}\frac{dT}{dx}\right) \times 10^{-8}, \tag{18}$$

where $-(1/\rho)(dT/dx)$ is the mass stopping power (S) of the target material (in MeV g^{-1} cm^2).

By comparing the charge Q_F collected in the Faraday cup with the charge Q_I collected in a large area ionization chamber (i.e., through which the entire beam passes), one can obtain directly the specific ionization p (in ion pairs per centimeter) for the beam of particles used and for the gas employed in the ionization chamber from the expression

$$Q_I = Ndpe \tag{19}$$

where N is the number of particles that pass through the ionization chamber with electrode spacing d in centimeters. (This formula is based on the assumption that the particles pass straight across the gap, without scattering.) If the same number of particles N is collected in the Faraday cup, Eqs. (15) and (19) give

$$\frac{Q_I}{Q_F} = \frac{pd}{z} . \tag{20}$$

The specific ionization p is related to the specific energy loss of the particle by

$$p = -\frac{1}{W}\frac{dT}{dx} , \tag{21}$$

where W is the energy required to form an ion pair in the ionization-chamber gas.

Equation (20) can be rewritten as

$$\frac{Q_I}{Q_F} = -\frac{d(dT/dx)}{zW} . \tag{22}$$

Hence, the ratio Q_I/Q_F is proportional to the ratio (dT/dx/W). If the specific energy loss of the incident particles is known, the value of W for the particular beam used and for the particular gas in the ionization chamber can be determined from this ratio. If not, the specific energy loss can be determined from the measured ratio Q_I/Q_F with a given value of W.

Because the Faraday cup must be thick enough to stop the primary particles, as well as their secondaries, the physical size required for proton energies greater than, say, 400 MeV makes the use of a Faraday cup less attractive. In applications in which the entire energy of the particles is expended in the target, the target itself may constitute the Faraday cup, if it is electrically conducting.

C. Secondary-Emission Monitor

The secondary-emission monitor (SEM) is particularly useful in high-intensity radiation fields where ionization chambers cannot be used because of incomplete ion collection due to recombination (Tautfest and Fechter, 1955). In a SEM the charge collected is due to the transfer of low-energy secondary electrons between the high-voltage electrode and the collection electrode, in ultrahigh vacuum ($\approx 10^{-8}$ torr). Greening (1954) first explained the principle of operation of such a vacuum "ion chamber," and a brief review will be found in Chapter 9, Section V, K (Volume II). The response of the SEM is linear with particle flux (number of particles per unit time).

A typical SEM, used at the Berkeley cyclotrons to monitor intense beams of heavy charged particles, contains an alternating stack of high-voltage foils and collection foils of aluminum, as shown in Fig. 11.

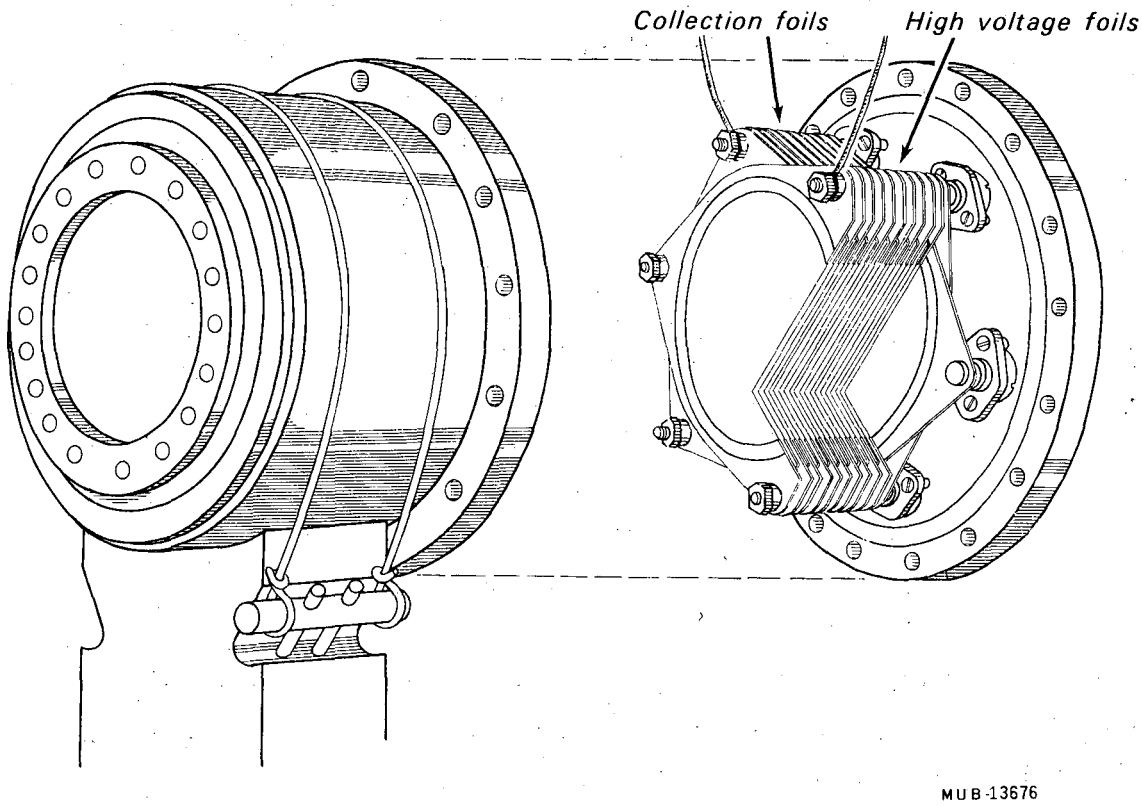

Fig. 11. Exploded view of a secondary emission monitor (SEM).

The vacuum chamber is constructed of stainless steel with aluminum foils and aluminum vacuum windows. The standoff insulators and feed-through insulators are of a ceramic material. The aluminum foils are held between two support rings which have engaging grooves. Adjacent sets of rings are supported on alternate mounting studs. When the foil assembly is axially tightened the foils are held taut. The aluminum vacuum foils forms a metal-to-metal seal with the stainless steel chamber. Prior to assembly, all stainless steel parts are electropolished to produce smoother and cleaner surfaces. The assembled chamber is baked under vacuum at 200°C for several days. The vacuum is maintained with a Vac-Ion pump (Varian Associates, Palo Alto, California), and is operated at a residual pressure of about 2×10^{-9} Torr.

This monitor can be used to obtain reproducible results if the foil surfaces are kept free of adsorbed materials, which may affect the emission of secondary electrons.

The yield, δ, of emitted electrons per incident particle can be expressed as

$$\delta = \frac{dT/dx}{\epsilon} \Delta x , \tag{23}$$

where ϵ is the average energy required to produce one emergent electron and Δx is the thickness of the region in which the escaping electrons are produced (Oda and Lyman, 1967; Lyman, 1967).

Since most of the emitted electrons have a very low energy (< 10 eV), they must be produced very near the surface. The total yield of the monitor depends more on the number of surfaces than on the thickness of the foils (since for most of the electrons emitted Δx is much smaller than the thickness of a single foil). The relative number of electrons transferred between the two sets of foils per incident particle, as a function of applied voltage, is shown in Fig. 12. The response of the SEM can be calibrated by means of a Faraday cup, or by an ionization chamber under beam and voltage conditions such that current saturation can be adequately achieved.

The SEM current, as a function of the thickness of absorber placed in front of the SEM, it very similar to that of an ionization chamber (see Section IV, A); that is, the response curve looks very much like a Bragg curve.

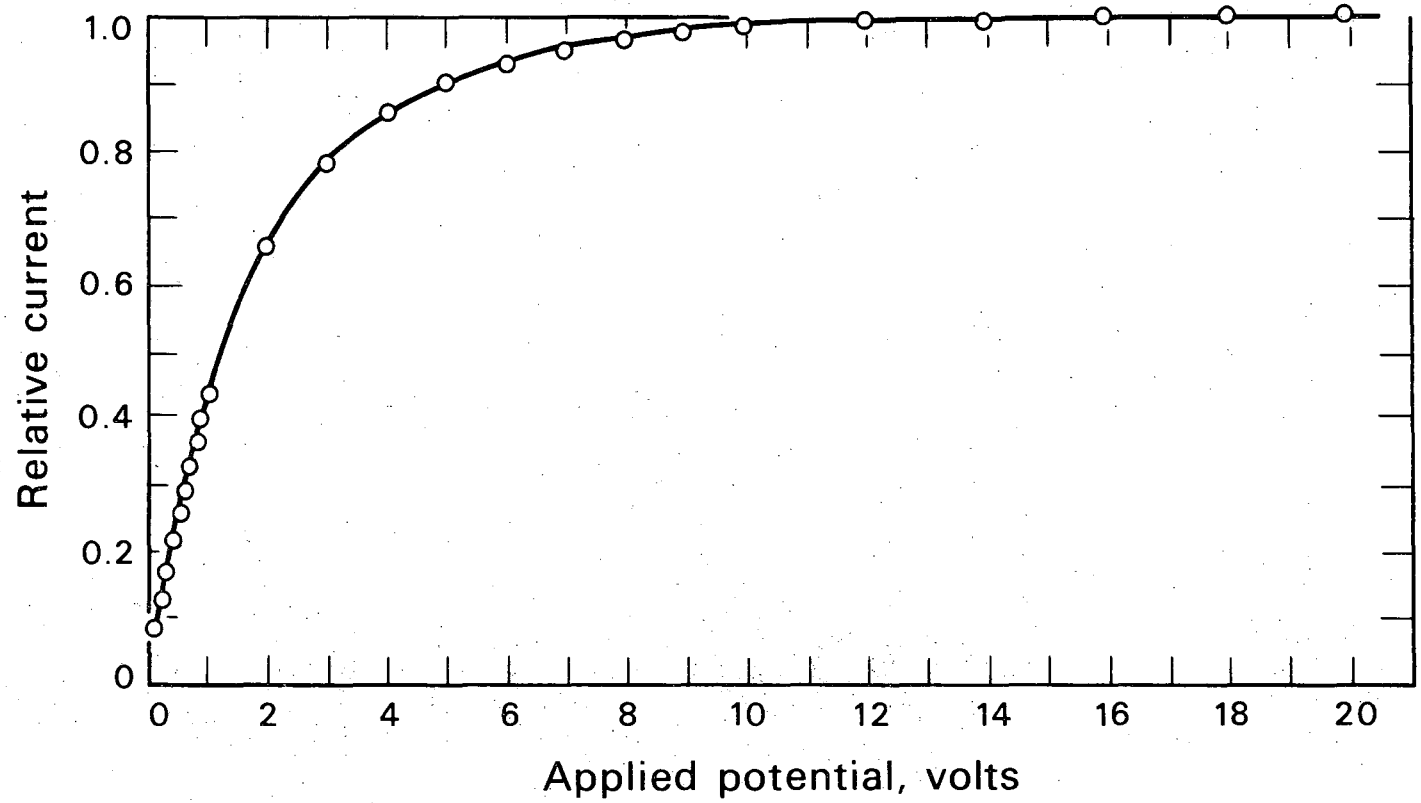

Fig. 12. Saturation curve (i.e., current collected versus applied voltage) for a secondary emission monitor of the type shown in Fig. 11.

D. Activation Dosimeter

Heavy charged particles produce radioactive isotopes by inelastic nuclear interactions. The induced activity of the sample may be used to determine either the particle flux (particles/sec) in the entire beam, or the particle flux density (particles/cm^2-sec) within a small area of the beam, depending on the geometric arrangement of the irradiation. Activation analysis with charged particles has been extensively treated by Tilbury (1966). The general techniques and computational approach are similar to those encountered in neutron-activation dosimetry, as discussed in Chapter 21, although the interaction cross sections differ, of course.

If a sample is irradiated at a given constant level of particle flux density ϕ for a time that is very long compared with the half-life of the radioactive species produced, the rate of decay A_∞ (disintegrations/sec) finally reached equals the rate of production of the radioactive atoms. A_∞ is called the "saturation" activity level. Usually the irradiation time t' is more limited in extent, and one must derive the value of A_∞ from the actual activity $A(t')$ achieved at the end of the exposure. This in turn must be gotten from a counting measurement, performed at some time t seconds after the irradiation is completed, using a counting apparatus (for detecting the appropriate emitted γ ray, β ray, or other particle) which has an overall efficiency of ϵ counts per disintegration. The value of A_∞ is obtained from

$$A_\infty = \frac{A(t')}{(1 - e^{-\lambda t'})} = \frac{C(t', t, \epsilon)}{\epsilon e^{-\lambda t}(1 - e^{-\lambda t'})}, \qquad (24)$$

where λ is the decay constant (sec^{-1}) of the radioactive product, and $C(t', t, \epsilon)$ is the measured counting rate.

Since A_∞ is equal to the rate (reactions/sec) at which the radioactive atoms are being produced by the particles passing through the sample, the particle flux density ϕ (assumed homogeneous over the sample) can be derived from A_∞ by

$$\phi = \frac{A_\infty}{N\sigma} = \frac{A_\infty M}{mn\sigma N_A}, \qquad (25)$$

where ϕ is in particles per cm^2 per sec; N is the total number of target nuclei in the sample; σ is the reaction cross section (i.e., number of reactions per target nucleus per incident particle/cm^2); M is the molecular

weight of the sample material (g/mole); N_A is Avogadro's number, 6.023×10^{23} molecules/mole; m is the sample mass (g); and n is the number of target nuclei per molecule of sample material.

If, instead of the charged-particle beam's covering the sample, the entire beam is passed perpendicularly through a larger-diameter sample foil of uniform thickness, then the total particle flux ϕ_t can be obtained from

$$\phi_t = \frac{A_\infty}{N'\sigma} = \frac{A_\infty M}{\xi n \sigma N_A}, \tag{26}$$

where ϕ_t is in particles per second; N' is the number of target nuclei per cm^2 of sample foil area; σ is the reaction cross section [i.e., number of reactions per incident particle per target-nucleus/cm^2], and ξ is the foil thickness in g/cm^2.

One of the most common activation dosimeters utilizes the $^{12}C(p, pn)^{11}C$ reaction (Cumming, 1963; Measday, 1966; Tilbury, 1966). The γ radiation from annihilation of the positron from ^{11}C (half-life = 20.5 min) is counted, usually with a scintillation detector. Polyethylene (CH_2) is usually employed as the carbon-bearing foil; in this case n = 1 and M = 14.027 in Eqs. (25) and (26).

The induced ^{11}C activity in the body has been measured by a whole-body counter, for human subjects who had received a therapeutic dose of protons or helium ions (Sargent, 1962). Some of the ^{11}C produced ends up in carboxy-hemoglobin, and part of this is exhaled as ^{11}CO. Other useful radioisotopes produced in irradiating tissue are the positron emitters ^{13}N (half-life = 9.96 min) and ^{15}O (2.107 min). Activation dosimetry may be used to verify dose actually received by a biological test object in vivo.

E. Semiconductor Detector

Semiconductor detectors, solid-state analogs of ionization chambers, are discussed in Chapter 14 (Volume II). In semiconductors the charge carriers are electrons and holes. The use of a solid as a detector is attractive because the sensitive layer can be very thin, giving good spatial resolution in depth, while still absorbing enough energy to give good sensitivity. The latter characteristic is further enhanced because of the small amount of energy required to produce an electron-hole pair ($\approx$ 3.75 eV in silicon)(Goulding, 1965). Nearly 10 times as much charge is released for a given energy loss in silicon as in a gas. This leads to smaller statistical fluctuations in the number of

electron-hole pairs and, hence, improved energy resolution over that of gas-filled and scintillation counters having comparable energy absorption. The collection time for the charge produced by the ionizing radiation in the semiconductor detectors is very short, because of the high mobility of carriers in the electric field and the small distance between the electrodes. An attractive feature of these detectors is that their response is proportional to the deposited energy, independent of the particle. Their use for measuring energy and energy loss are discussed in the next section.

IV. MEASUREMENT OF HEAVY CHARGED-PARTICLE BEAMS

A. The Bragg Ionization Curve

A Bragg curve is a plot of the relative specific ionization of a collimated beam of particles, plotted as a function of the thickness of absorber that the beam has traversed. It can be obtained experimentally by taking the ratio of current from two ionization chambers, as shown in Fig. 13. A monitor chamber is placed ahead of a variable absorber, and a second chamber is placed behind the absorber. The shape of a Bragg curve is dependent upon many factors, mainly the energy and the energy spread of the initial beam, the nature of the incident particle, and the nature of the absorbing material. Since the amount of straggling increases almost linearly with the thickness of absorber, monoenergetic beams of low energy show the sharpest Bragg peaks.

In Bragg-curve measurements, secondary particles from collimators used to define the beam should not contribute to the ionization in the second ionization chamber. In addition, the second ionization chamber, which detects the transmitted beam from the variable absorber, should have a collecting electrode with diameter large enough to cover the entire area of the transmitted beam; otherwise a different experimental curve is obtained. This curve is called the central-axis depth-dose distribution curve, which is useful for some purposes. Such curves for beams of protons and helium ions of several energies are shown in Fig. 14.

The dose delivered to the medium at the beam entrance surface may be called the "plateau dose," and the dose at the Bragg peak the "peak dose." The physical parameters of primary interest are the peak-to-plateau ratio and the width of the Bragg peak. The peak-to-plateau ratio is a very sensitive function of momentum spread (the same effect as energy spread) of the beam. With increasing momentum spread, the peak-to-plateau ratio is reduced considerably, with concomitant increase in the width of the Bragg peak. With

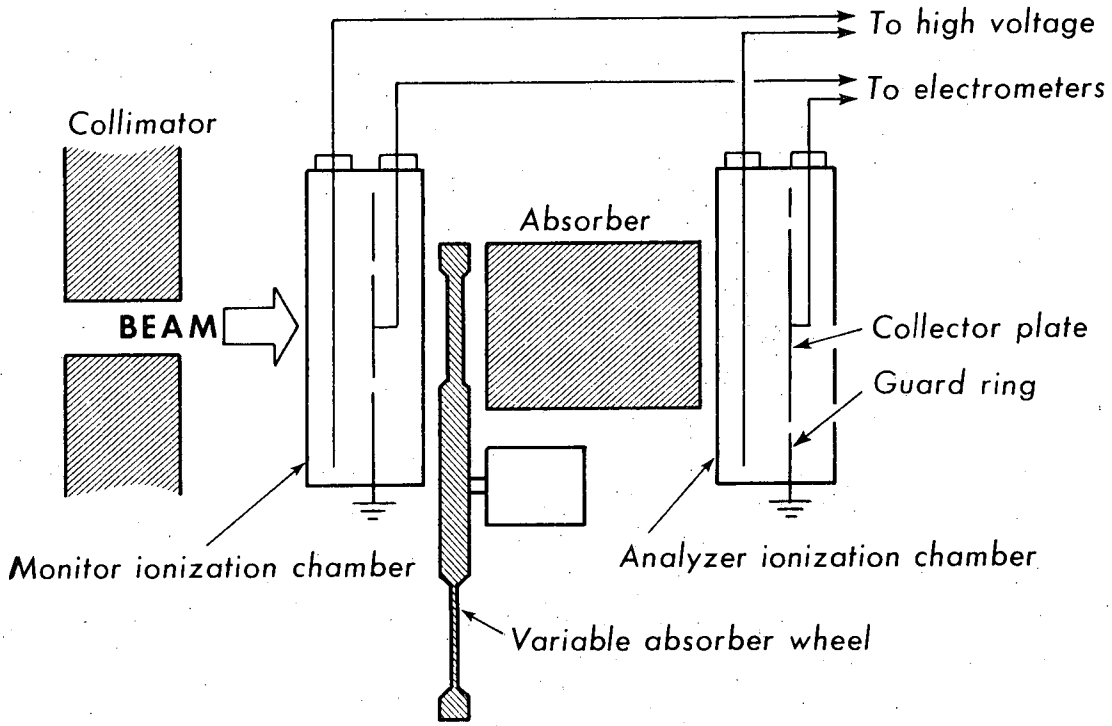

Fig. 13. Experimental arrangement for measuring the Bragg curve.

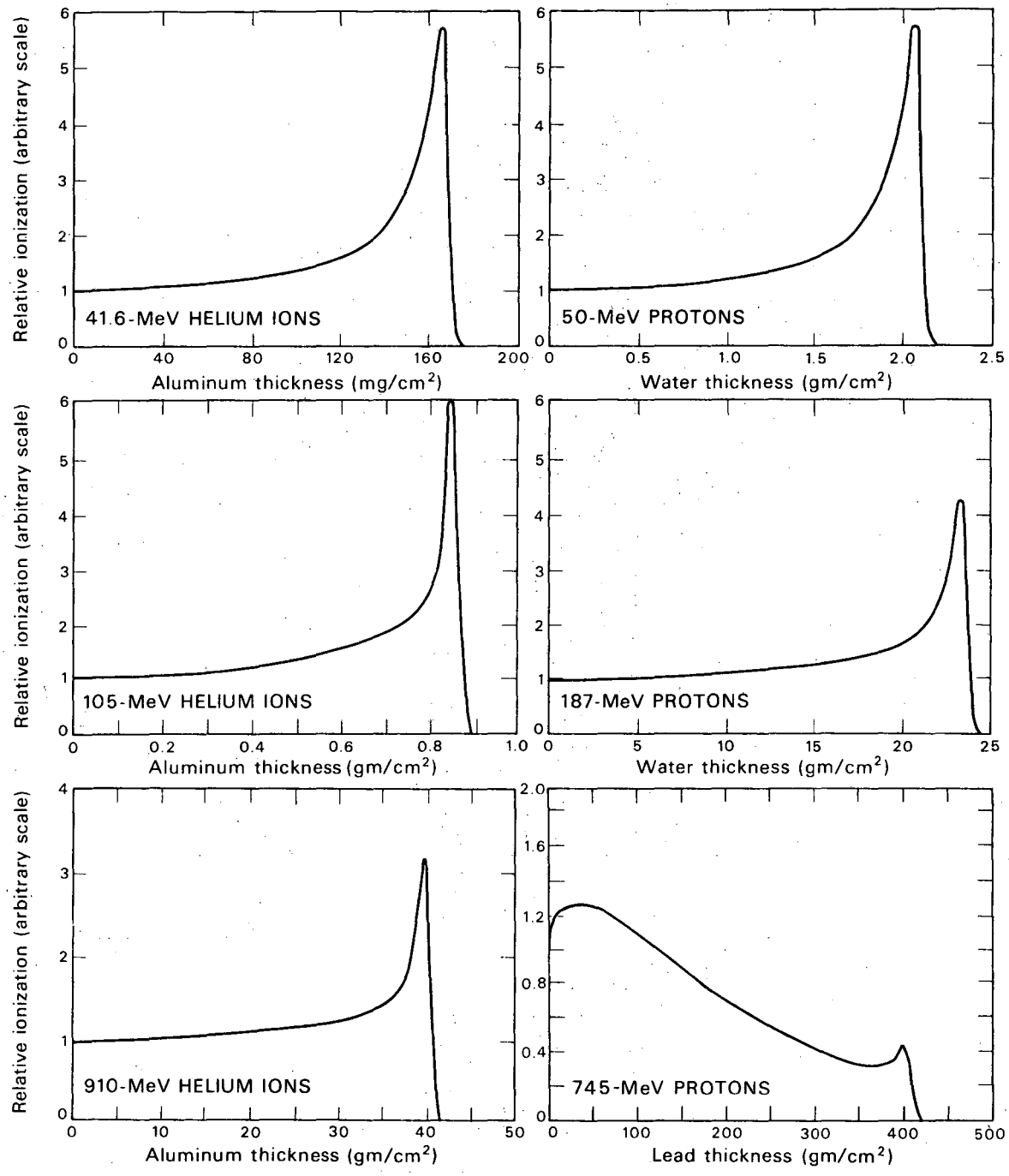

DBL 6711-1885

Fig. 14. Depth-dose distribution of proton and helium ion beams. The depth-dose distribution of a high-energy proton beam (730 MeV) in copper is very different in shape from the other curves. The initial dose buildup is due to secondary-particle production, and the reduction of dose with depth is due to loss of particles through nuclear interactions as described in the text.

increasing energy and hence increasing range of the particles, the range straggling increases. This effect reduces the peak-to-plateau ratio and broadens the peak of the curve. In addition, with increasing energy of the particles more particles are removed from the beam because of nuclear interactions (see Section II, 3) before they reach the Bragg peak, and this also results in a reduction in peak-to-plateau ratio. A computer program for calculating Bragg curves for heavy-ion beams is available (Litton, 1967).

Shown in Fig. 15 are Bragg curves of various heavy-ion beams in aluminum, all with initial energy of 10.4 MeV/amu. At zero absorber thickness the particle velocities are the same, and hence the square of the effective charge of the heavy ions is proportional to the specific ionization.

A differential type of ionization chamber may be used to determine the position of the Bragg peak and also to check the changes in the beam energy (Larsson, 1961; Hanna and Hodges, 1965). The collecting electrode is located between two high-voltage electrodes maintained at opposite polarity. If the first foil is negative with respect to the second, a positive signal is obtained from the collector electrode when the absorber is less than that needed to attain the peak. The exact location of the peak is determined by the amount of absorber needed to make the response of the two halves of the chamber equal but of opposite magnitude, thereby obtaining a null reading. Beyond the Bragg peak a negative signal is obtained from the ionization chamber until the absorber is thick enough to stop the beam completely. The large-area ionization chamber shown in Fig. 9 can be operated in this way.

B. Beam Profiles and Isodose Contours

For many applications of heavy-charged-particle beams, one needs to know the three-dimensional dose distribution in the irradiated material. For such measurements, the sensitive area of the detector should be kept small relative to the cross section of the beam. At the same time the detector must have adequate sensitivity. Small semiconductor devices are suitable for this application. An example of such a semiconductor device is a miniature silicon diode 0.1 cm in maximum diameter and 0.22 cm long (Koehler, 1967a; Raju, 1966).

The sensitivity of these diodes is found to decrease as the dose increases, owing to radiation damage. This, however, need not be a limitation on their use as radiation dosimeters. If the diode is preexposed to high radiation doses, of the order of 10^6 rads, the sensitivity of the diode is reduced

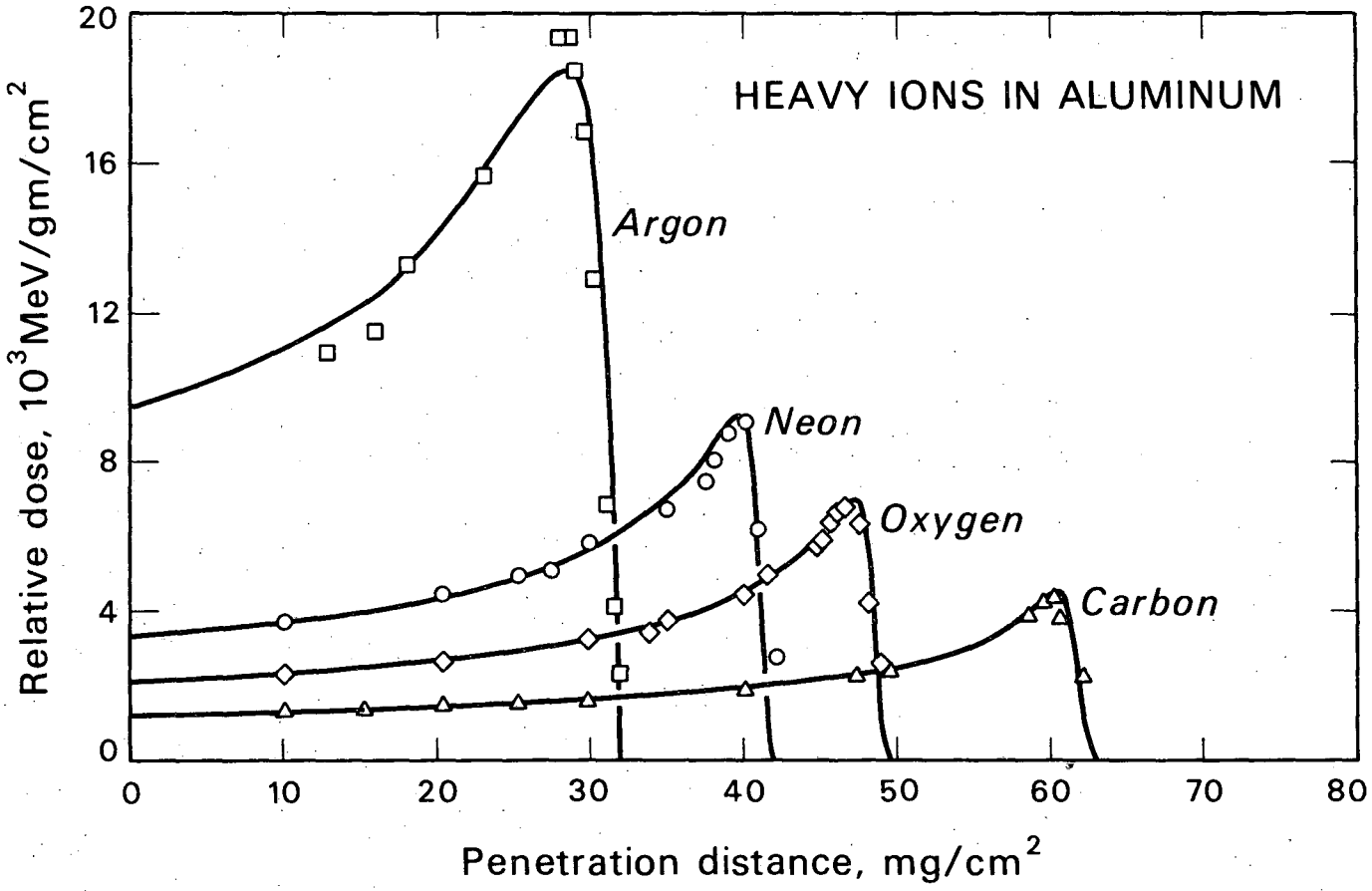

DBL 6712-1909

Fig. 15. Bragg curves of ^{10}Ar, ^{20}Ne, ^{16}O, and ^{12}C ions of initial energy 10.4 ± 0.2 MeV/amu, measured in aluminum. Solid curves are theoretical (Litton, 1967); points are experimental.

to about a third, but the sensitivity does not change significantly thereafter with further radiation exposures. The current generated in such a diode is proportional to the dose rate (Koehler, 1967a).

Figure 16 shows a set of profiles of a 127-MeV proton beam incident on water, as measured by a miniature silicon diode (Preston and Koehler, 1968). The measured distributions are nearly Gaussian in form. These experimental results are in good agreement with the theory of multiple scattering of heavy charged-particle beams as discussed in Section II, 4.

Profiles can also be measured by using ionization chambers, particle counters, photographic film, activation analysis, thermoluminescent dosimeters, and so forth. From a series of beam profiles, a set of isodose contours can be constructed. Figure 17 shows such an isodose plot for a degraded 910-MeV helium-ion beam in water.

If the profile itself is changing with time, continuous display of the profile is necessary (Jackson et al., 1959; Bewley et al., 1967).

C. Integral Range Curves

A plot of the number of particles that passed through an absorber as a function of absorber thickness is called an integral range curve or a number-distance curve. The number of charged particles that have passed through an absorber can be determined with particle counters such as Faraday cups. The experimental arrangement used to determine an integral range curve is similar to that shown in Fig. 13, but with the second ionization chamber replaced by a particle counter. For low-energy particles for which nuclear interactions can be neglected, the number of particles remains essentially constant from zero absorber to a thickness somewhat less than the mean range of the particles. This is illustrated in Fig. 18 for a number of heavy ions. At high energies, particles are lost from the beam by nuclear interactions. Under these conditions the integral range curve as shown in Fig. 19 for a 910-MeV helium-ion beam has a negative slope. An estimate of the cross section for these interactions, σ_R, can be obtained from this slope. Thus

$$\sigma_R = -\frac{1}{N_v \phi_t} \cdot \frac{d\phi_t}{dx} , \qquad (27)$$

where σ_R is given in reactions per incident particle per nucleus per square centimeter, N_v is the number of atoms per cubic centimeter of the absorber, ϕ_t is the total particle flux (particles/sec), and $d\phi_t/dx$ is the number of

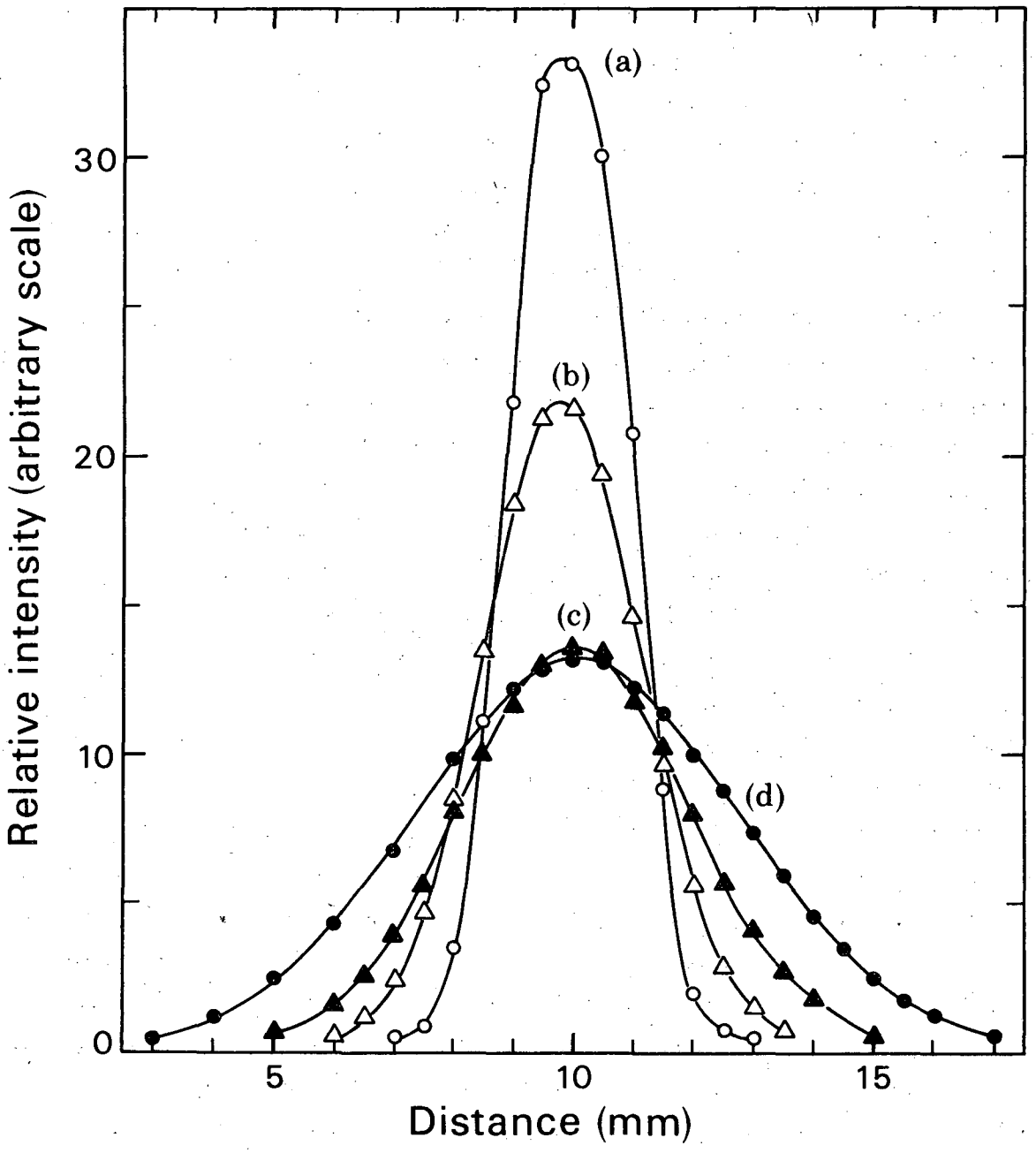

DBL 6711 1891

Fig. 16. Beam intensity as a function of position along a diameter of the beam, measured at (a) 0 cm, (b) 5.7 cm, (c) 8.7 cm, and (d) 11.4 cm depth of penetration in water. The incident energy is 127 MeV and the median range is 11.4 cm.

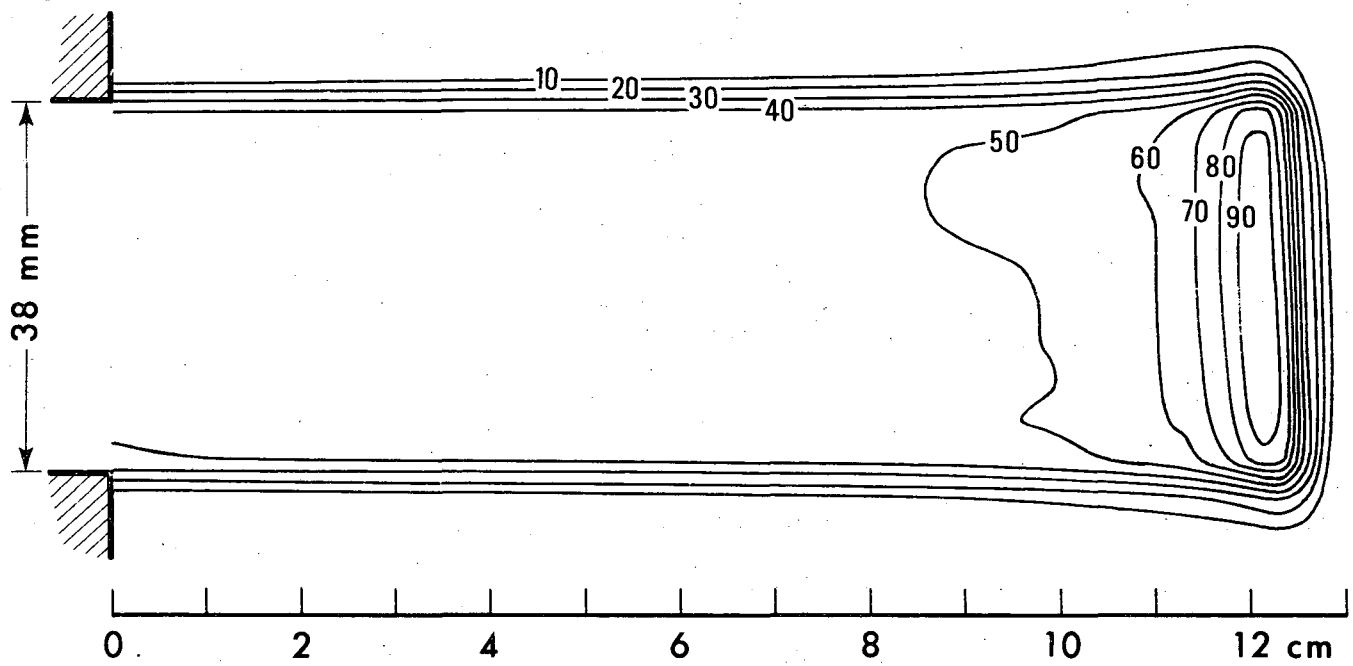

DBL 678-1717

Fig. 17. Isodose contours in water of a 910-MeV helium-ion beam, already degraded to ≈ 400 MeV by 32 mm of copper.

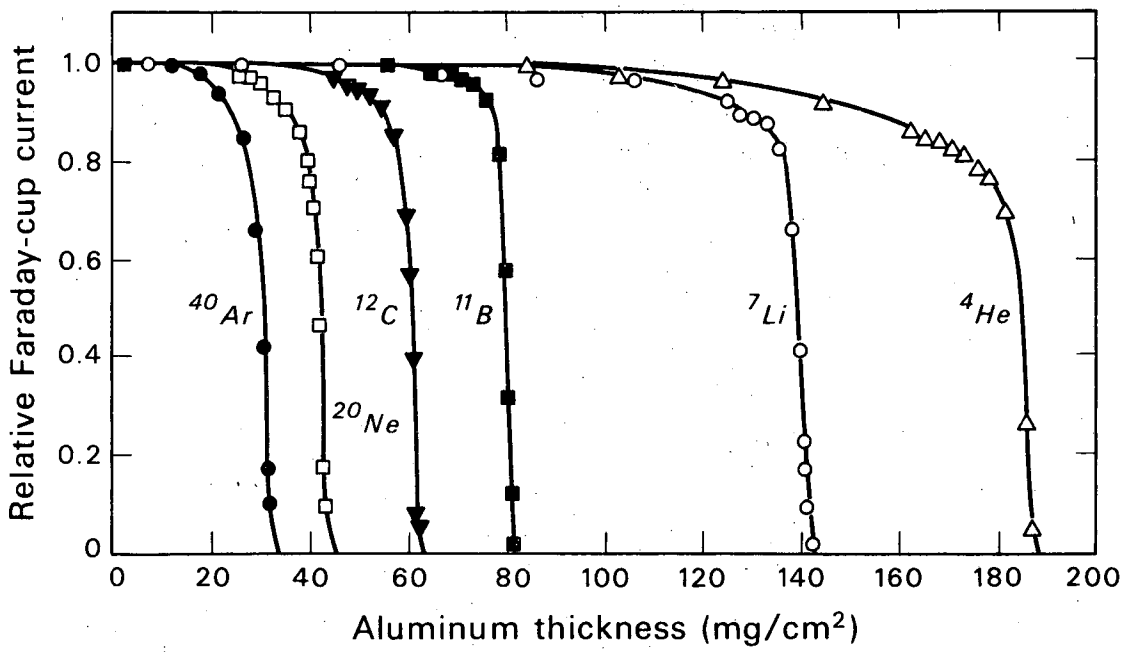

DBL 6711-1887

Fig. 18. Modified integral-range curve for various heavy ions of initial energy 10.4 ± 0.2 MeV/amu. Since the Faraday cup measures the total charge of the beam, the ordinate represents the product of the number of particles and the average charge per particle.

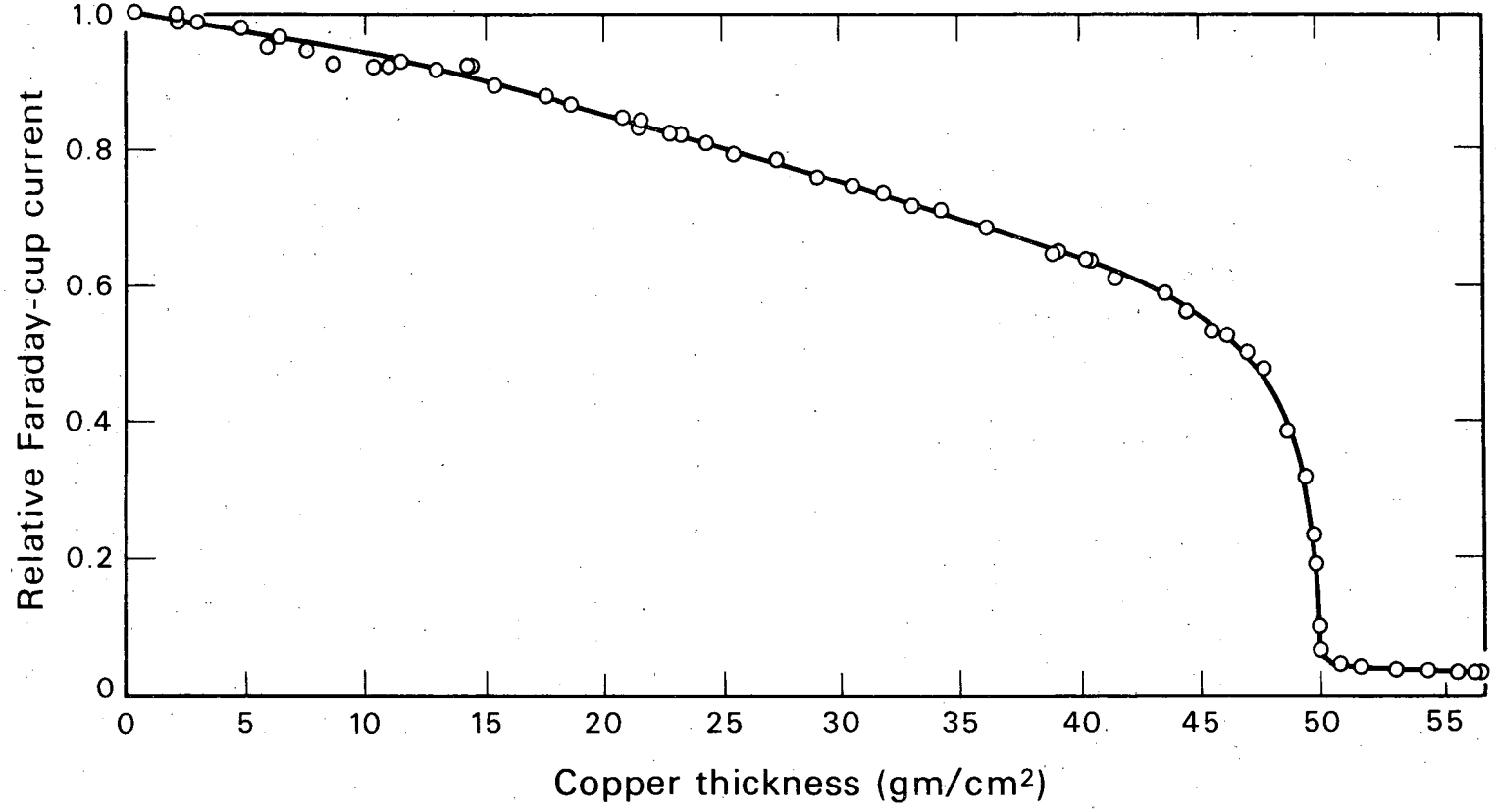

DBL 6711-1888

Fig. 19. Charge collected in a Faraday cup versus copper absorber thickness for a 910-MeV helium-ion beam. This is very similar to the number-distance curve, since the charge of these energetic ions remains essentially the same until the last few milligrams per square centimeter of the total range. Notice the slope to the left of the knee ($\approx$ 42 g/cm^2) resulting from nuclear interactions.

particles interacting (lost) per centimeter-second (i.e., the slope of the integral range curve).

In the energy region between a few MeV/amu and a few GeV/amu, σ_R is approximately

$$\sigma_R \approx \pi r_0^2 \left(A_T^{1/3} + A_I^{1/3}\right)^2 \left(1 - \frac{V_c}{T_{c.m.}}\right), \tag{28}$$

where r_0 is the nuclear radius, A is the atomic weight, the subscripts T and I refer to the target and incident nuclei respectively, V_c is the Coulomb-barrier potential, and $T_{c.m.}$ is the total kinetic energy in the center-of-mass system. Here r_0 is about 1.3×10^{-13} cm for protons and light nuclei of a few MeV per nucleon. At high energies the nuclei become partially "transparent" and the effective radius becomes smaller. Measurements are needed to determine the exact energy dependence of r_0. The V_c (in MeV) is given by

$$V_c = 0.96 \frac{Z_T Z_I}{A_T^{1/3} + A_I^{1/3}}, \tag{29}$$

where Z is the atomic number and the subscripts are as defined before.

Calculations indicate that for proton energies from 0 to 400 MeV the dose contribution from secondary particles heavier than protons, produced by nuclear interactions, generally does not exceed 2.5% of the total dose in tissue (Turner et al., 1964; see also Blosser et al., 1964; Wheeler, 1966). The biological effect of heavy recoils may be more important than their dose contribution would indicate, since the heavy recoils may have a very high relative biological effectiveness (Jung, 1967; Zimmer, 1966).

An estimate of the range of the particles can be obtained by considering the tail of the integral range curve (Santoro, 1965; Santoro et al., 1966). A useful reference point is the extrapolated range, which can be obtained by drawing the tangent to the integral range curve at the point of steepest slope and extrapolating it to the horizontal axis.

D. Energy-Loss Measurements

In most of the studies relating biological damage to the energy loss of the particles, the experimenter usually has had to rely on theoretical calculations of the energy loss. However, in many of the biological experiments,

the theoretical calculations may not be adequate and can profitably be supplemented with experimental measurements. For example, in the low-energy region where electron pickup becomes important, one needs experimental data on effective charge (Heckman et al., 1960; Northcliffe, 1960; Schambra et al., 1960; Roll and Steigert, 1960). In the high-energy region where production of secondary particles by nuclear interactions is important, it becomes increasingly difficult to predict the relative contribution of all the secondary particles. In addition, whenever there is an uncertainty in energy spread of the primary particles, it is difficult to calculate the energy loss.

Semiconductor detectors possess several useful properties for energy-loss measurements. If the sensitive layer of the detector is made thin enough, the energy deposited in it by a particle will be small compared with the energy carried by the particle. The detector can then be used to measure energy-loss distributions. On the other hand, if the detector is thick enough to stop all the particles in the beam, it can be used to measure the energy distribution of the particles (Raju, 1967).

When an energetic charged particle passes through a detector, it loses energy by a series of collisions with the electrons of the detector material. As a first approximation, the probability of an energy loss in a single electron collision is proportional to ϵ^{-2} (Landau, 1944), where ϵ is the energy imparted to the electron. Thus collisions resulting in a large energy transfer to an electron are relatively infrequent compared with small-energy-loss collisions. However, these large-energy-loss collisions account for a significant proportion of the total energy transfer. This phenomenon has been theoretically investigated by Landau (1944), Symon (1952), Vavilov (1957), and others; it is often called the Landau effect. Experimental investigations have been carried out by Gooding and Eisberg (1957), Rosenzweig and Rossi (1963), and Grew (1965), all of whom compared their data with the theoretical data of Symon.

In Vavilov's treatment, the dimensionless parameter κ is introduced.

$$\kappa = 0.150 \frac{(\xi Z z^2)}{(A)} - \frac{(1 - \beta^2)}{(\beta^4)}, \qquad (30)$$

where ξ is the thickness of the detector (in g/cm^2); Z is the atomic number of the detector material; A is the atomic weight of the detector material; z is the charge on an incident particle; and β is the velocity of an incident

particle divided by the velocity of light in vacuum. Here κ may be thought of as a measure of the ratio of the mean energy loss to the maximum possible energy loss in a single collision.

When the parameter $\kappa >> 1$, the fluctuations are negligible and the resulting total energy-loss distribution curve is approximately Gaussian. Here the average energy loss equals the most probable energy loss. If, on the other hand, $\kappa << 1$, the fluctuations are large; then the resulting energy-loss distribution curve would have a characteristic high-energy tail, thereby deviating considerably from a Gaussian distribution. In this case, the most probable energy loss is less than the average energy loss, as shown in Fig. 20. Note also that the full width at half-maximum is approximately 30%; this is typical of situations with fast particles passing through thin detectors. These experimental measurements of energy-loss distributions are in good agreement (Maccabee, 1966; Maccabee et al., 1966; Maccabee and Raju, 1968) with the rigorous theory of Vavilov as tabulated by Seltzer and Berger (1964). If one considers the thickness of the sensitive target in a biological sample to be equivalent to the detector thickness ξ of Eq. (30), then one can see that κ will be $<< 1$ for most charged particles, and therefore there will be a broad distribution of energy-loss values within the target. If the target is small (e.g., nuclei and molecules), there may be too few collisions for the Landau theory to be valid. One must then use Poisson statistics and compensate for δ-ray escape.

E. Energy Measurements

Fluctuations of the energy lost in a given small thickness result in fluctuations in the total thickness traversed by the individual particles, that is, range straggling, as discussed earlier. The consequence of this effect is that the residual energies of the particles at the Bragg-peak position have a wide spectrum. Figure 21 illustrates this effect for a 50-MeV proton beam in aluminum (top curve) and for a 910-MeV helium-ion beam in copper (bottom curve). A lithium-drifted silicon detector was used in obtaining these data (Raju, 1967). The corresponding LET values in water are also shown in that figure. Note that the modal energy at the Bragg peak is much higher than one might expect; thus the LET is correspondingly lower. These measurements, together with those at the Harvard cyclotron (Koehler, 1967b), indicate that one can use as a general rule of thumb that the most probable energy at the Bragg peak is about 10% of the initial kinetic energy.

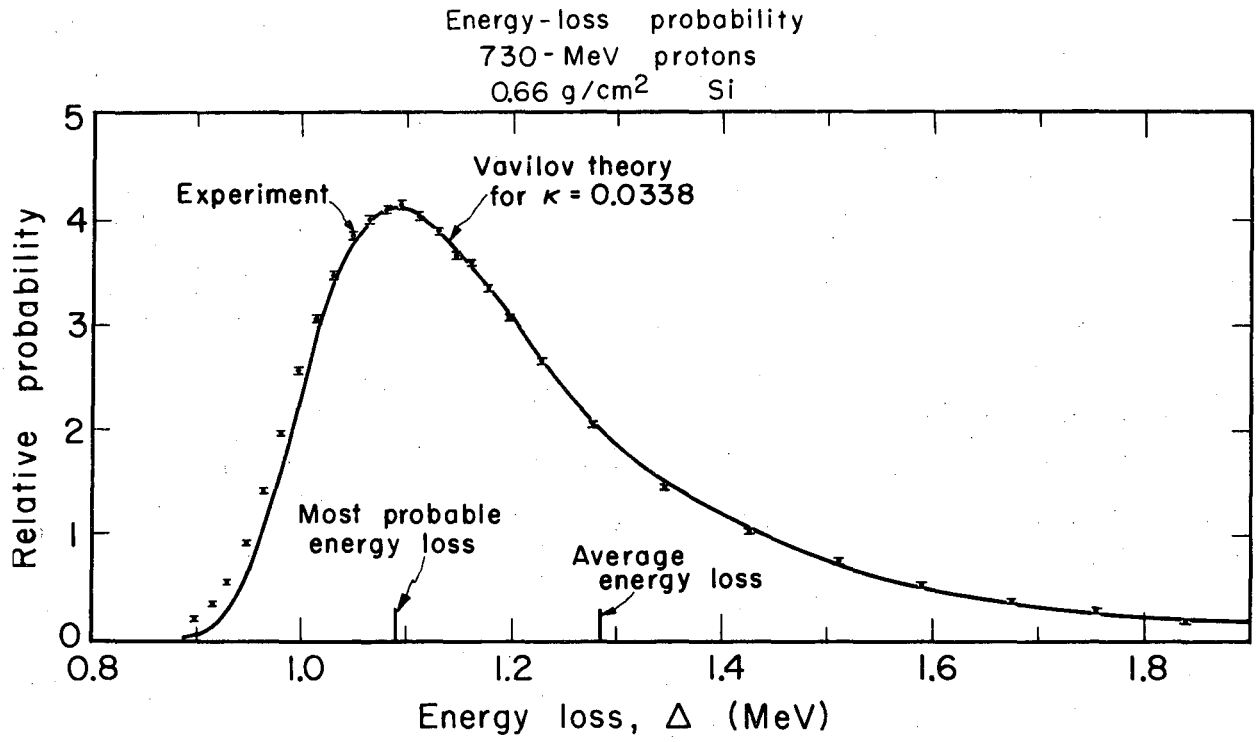

Fig. 20. Energy-loss probability, 730-MeV protons in 0.66-g/cm^2 silicon; κ = 0.0338 (Maccabee et al., 1966).

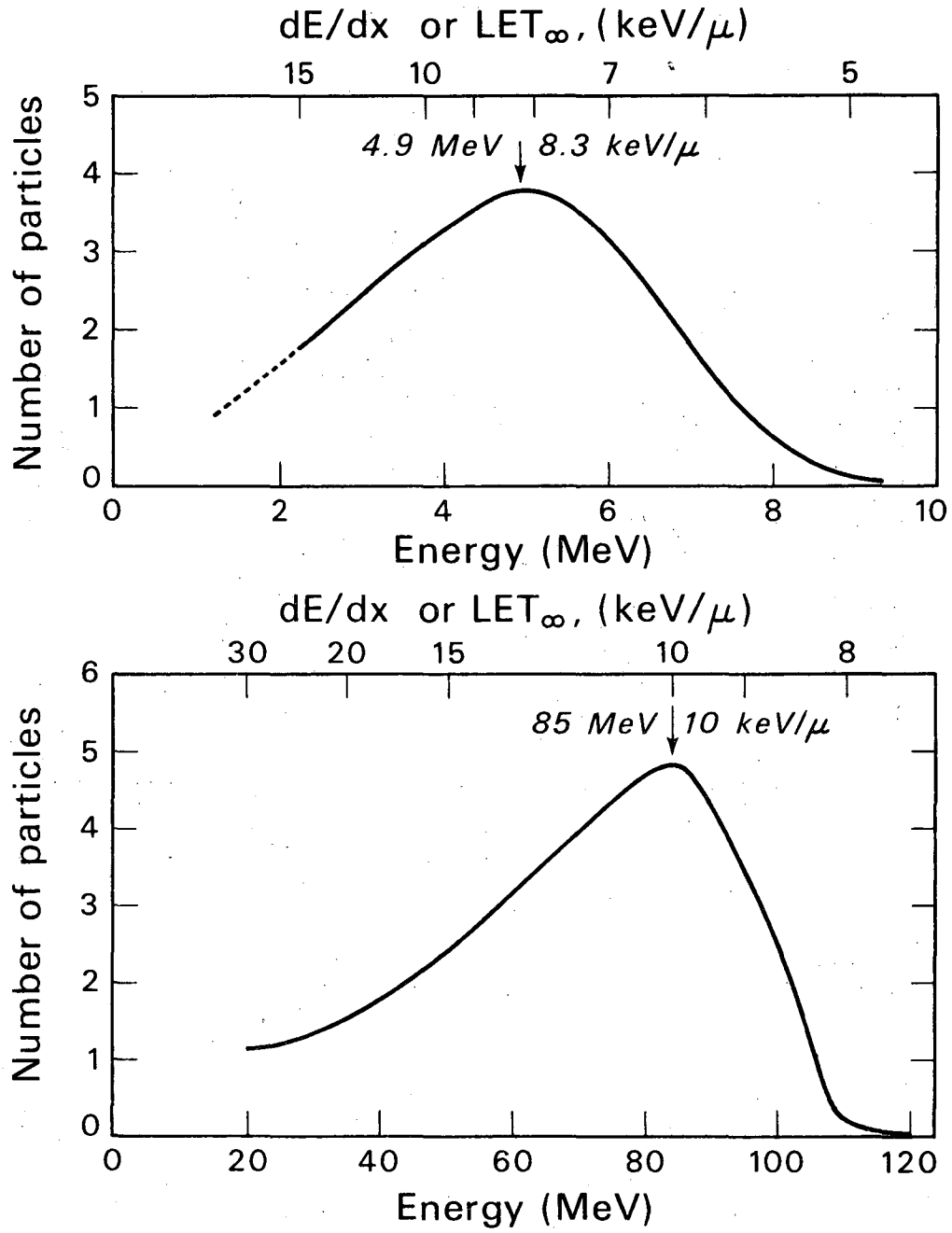

DBL 6712-1908

Fig. 21. Energy distribution of charged particles at the Bragg peak, as measured with a lithium-drifted silicon detector (Raju, 1967). The upper curve is for a 50-MeV proton beam in aluminum; lower curve is for 910-MeV helium ions in copper.

F. Dose Measurements with Semiconductor Detectors

Semiconductor detectors can also be used to measure the dose by integrating the pulses due to individual particles for low-intensity beams.

When a negative π^- meson is brought to rest in a medium, say tissue, it is captured by a constituent nucleus, which explodes into a "star" consisting of short-range and heavily ionizing fragments capable of delivering a large localized radiation dose. As a result, the Bragg peak at the terminal end of the track is considerably augmented. Because of the large range of energy deposition involved at the plateau and peak regions of negative π^- mesons, semiconductor detectors have been used to measure depth-dose distributions. In addition, these detectors have been very useful for getting information on ionization density at the Bragg peak (Raju et al., 1967).

When a positive π^+ meson comes to rest, it decays into a positive μ^+ meson, which in turn decays into a positron. Hence the dose is less concentrated spatially than for the π^--meson beam. Figure 22 shows the depth-dose distributions of π^+- and π^--meson beams of energy 96 MeV, as measured by a lithium-drifted silicon detector, illustrating this effect.

V. TECHNIQUES OF EXPOSURE

A. The Track-Average and Track-Segment Techniques

It has long been recognized that the radiobiological effects of ionizing radiation depend on the specific energy loss (i.e., linear energy transfer, or LET) of the particles in the biological samples (Lea, 1946; Timofeeff-Ressovsky and Zimmer, 1947; Zirkle, 1952). However, one rarely finds only radiation of a single LET present at a point of interest; almost always a distribution is present, and one must decide how to average it to obtain some meaningful characteristic LET for the distribution. Two methods of averaging have been used extensively: the track-average method and the track-segment method.

The track-average method applies when the thickness of the biological object in question is a large fraction of the particle range, or if random portions of different tracks pass through the object. This results in a wide spread in LET values, ranging from that characteristic of the lowest particle energy attained in the sample to a minimum value determined by the charge and maximum velocity of the incident particles. The heterogeneity of the specific energy-loss values increase if there is a nonuniformity of the initial particle energy, and becomes particularly pronounced for x-ray and neutron beams.

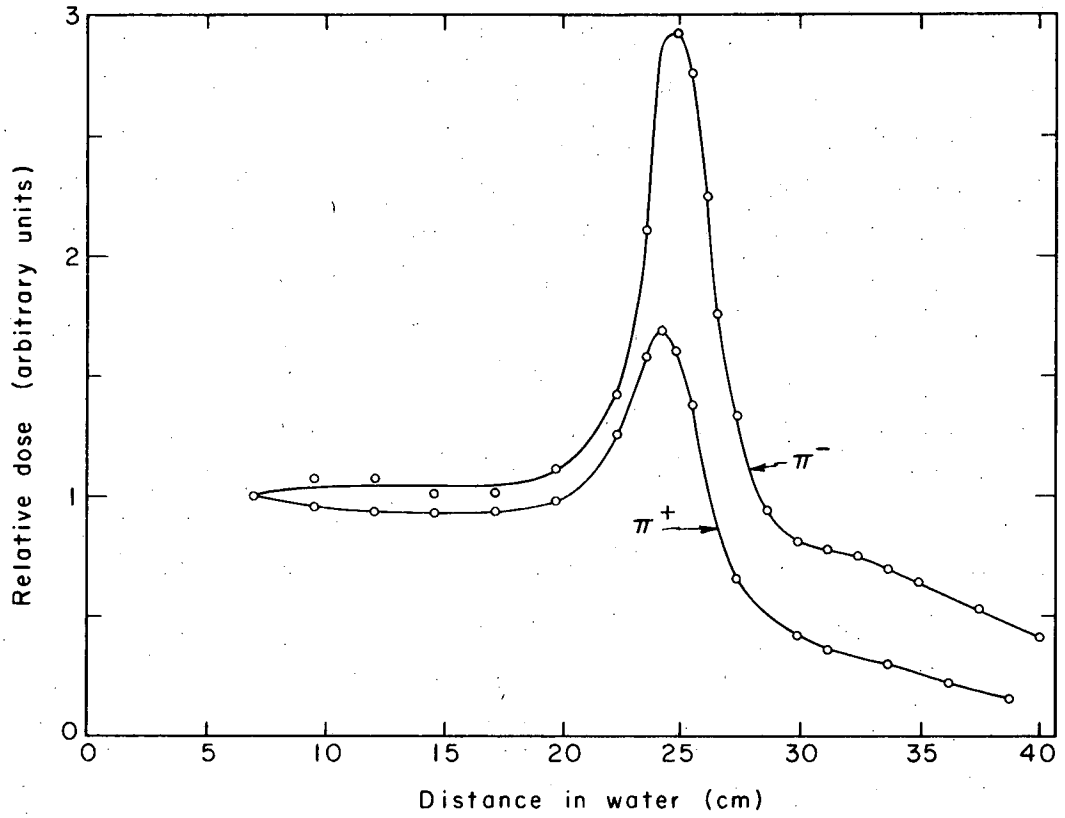

Fig. 22. Depth-dose distribution of 96-MeV π^+ and π^- meson beams.

The track-segment method, on the other hand, applies when the thickness of the biological sample is small compared with the range of a parallel monoenergetic particle beam. Here the samples are placed along the particle path at a point where the LET has been predetermined. Different LET values are obtained by utilizing different linear portions of the particle track in successive experiments. Another possibility is to expose a stack of thin samples sandwiched between thin absorbers, so that the total stack is thick enough to stop the particle beam. By analyzing separately the biological effects induced in each layer, one can study the effects of varying specific energy loss over the entire range attainable by the radiation in question (Pollard et al., 1955). The method enables one to obtain relatively narrow distributions of LET in each sample. However, the greatest variations in mean energy loss attained in this way are usually only about one order of magnitude with a given monoenergetic beam.

The Berkeley heavy-ion linear accelerator can produce monoenergetic beams of stripped nuclei up through atomic number 18 with energies of 10 MeV/amu. Different specific energy-loss values can be obtained in separate experiments by irradiating thin samples with particles of different atomic number but equal velocity. By this method the range of energy-loss values can be extended to cover more than three orders of magnitude. Furthermore, the fraction of the total energy deposition in the sample due to δ rays is constant, irrespective of the nuclei used, and since the ions have the same velocity, their δ-ray LET spectrum is the same (Howard-Flanders, 1958; Haynes and Dolphin, 1959). Nearly half the energy of the heavy ion is transferred to electrons that are capable of further ionization.

B. Ridge Filters

For some applications it is desirable to modify the depth-dose distribution normally obtained with a given heavy-charged-particle beam. Although this can be done by the superposition of beams with differing depths of penetration, it is sometimes desirable to produce a modified depth-dose distribution may be obtained by use of a composite absorber, called a "ridge filter" (Karlsson, 1964). Figure 23 shows the normal depth-dose distribution of a 187-MeV proton beam together with a modified depth-dose distribution and the ridge filter used for producing this modification. This type of filter consists of a series of similar units placed side by side to form a composite absorber whose cross section is larger than the beam area. Each unit is essen-

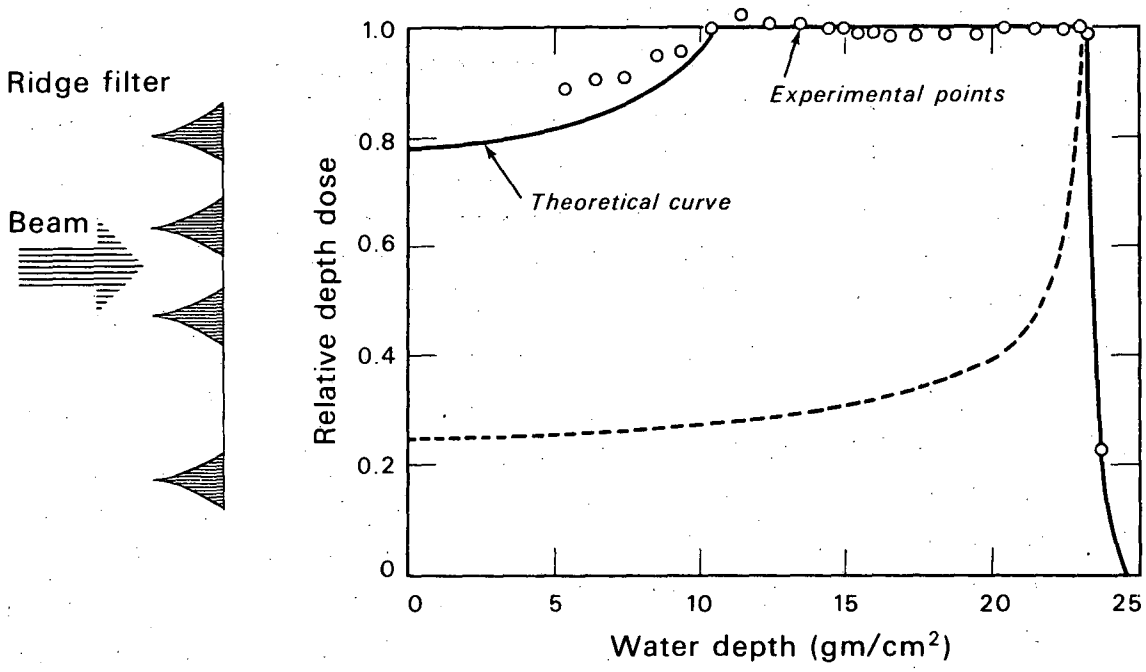

DBL 6711-1892

Fig. 23. Depth-dose distribution of 187-MeV proton beam in water, together with modified depth-dose distribution obtained by using ridge filter made of Hevimet (90% W, 7% Ni, and 3% Cu), redrawn from Karlsson (1964). The maximum thickness of the ridge filter is 13 mm, the base of each unit is 6 mm wide, and the units are separated by 2 mm.

tially a stepwise variable-thickness copper absorber. The width of an individual step determines the relative intensity, and the total thickness of the step determines the residual energy. The entire filter is oscillated on a line perpendicular both to the beam axis and to the length of the individual units of the ridge filter. Such a "flattened" depth-dose distribution is useful for a uniform irradiation of a large volume.

Unlike the depth-dose distribution of monoenergetic charged particles, the distribution resulting from a solar-flare exposure generally decreases exponentially with depth. However, it is possible to obtain the expotentially decreasing depth-dose distribution from monoenergetic charged-particle beams by using an appropriate ridge filter. Figure 24 shows the depth-dose distribution of a degraded monoenergetic 910-MeV helium ion beam, together with the modified depth-dose distribution and the ridge filter used for this modification.

C. Discrete Lesions

Various discrete lesions can be produced for experimental purposes in animal tissue, or for therapeutic purposes in man, by use of collimated narrow beams of high-energy charged particles. By utilizing the Bragg peak of such beams, a laminar lesion can be formed in a plane perpendicular to the beam direction at a depth determined by the range of the particles (Janssen et al., 1962; Malis et al., 1957). This technique as illustrated in Fig. 25 (Tobias, 1962) might be used to study the connections and functions of cerebral cortex (Malis et al., 1962). As the entrance dose is increased the lesion is extended toward the surface. The cross section of these lesions is determined by the size and shape of the beam-defining aperture. Very large doses produce lesions that extend all the way along the path of the beam (Van Dyke and Janssen, 1963). If the aperture is a narrow slit, the beam may be used to sever connections between adjacent structures (Van Dyke et al., 1962).

The shape of these lesions can be further modified by rotating the object during irradiation. In this manner, it is possible to make spherical, elliptical, or disk-shaped lesions at various depths (Leksell et al., 1960; Tobias, 1962). Small spherical lesions are most easily produced by rotating the irradiated object 180 degrees about an axis at right angles to the beam direction, and using the plateau portion of the heavy-charged-particle beam with a circular cross section. The production of such lesions has been utilized in the treatment of Parkinson's disease (Tym et al., 1965).

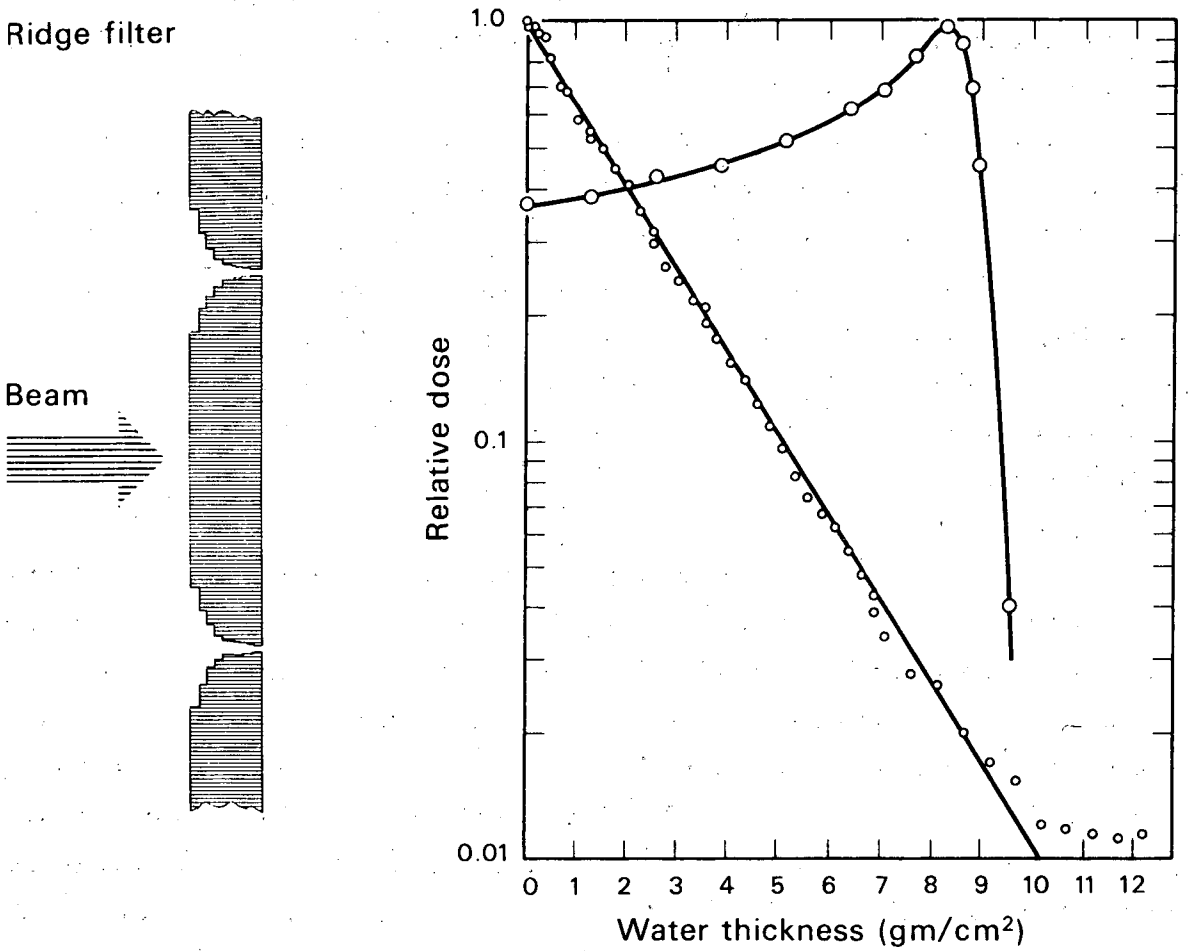

DBL 6711-1890

Fig. 24. Depth-dose distribution of degraded (38.1 mm of copper) 910-MeV helium-ion beam (large circles) together with modified depth-dose distribution obtained by using a copper ridge filter (small circles). The maximum thickness of the ridge filter is 14.3 mm, the width of an individual unit is 50.8 mm, and the separation between the individual units is 0.1 mm.

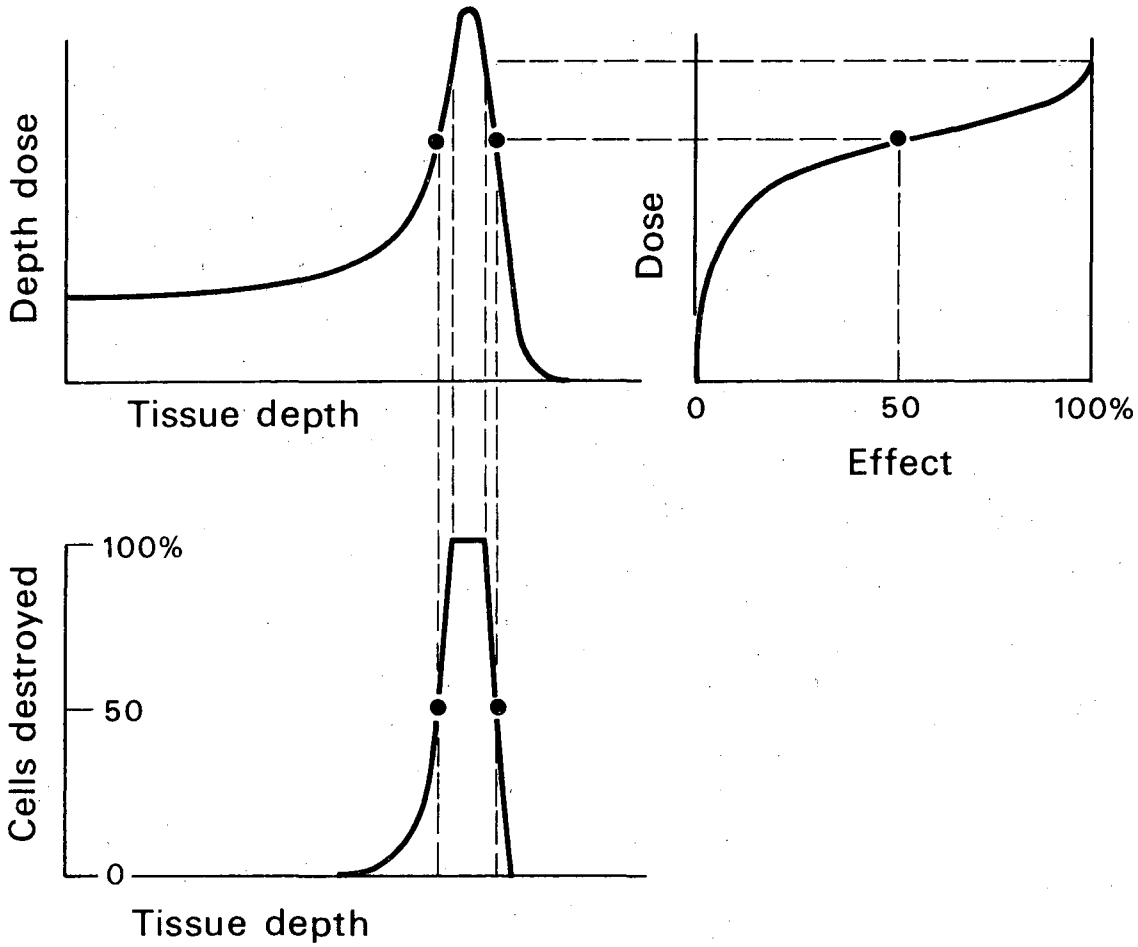

DBL 6711-1886

Fig. 25. Depth-dose distribution of heavy-charged-particle beam (upper left). On upper right is a hypothetical dose-effect relationship. Lower left shows the location and width of the laminar lesion; effects greater than 50% are assumed to produce a lesion.

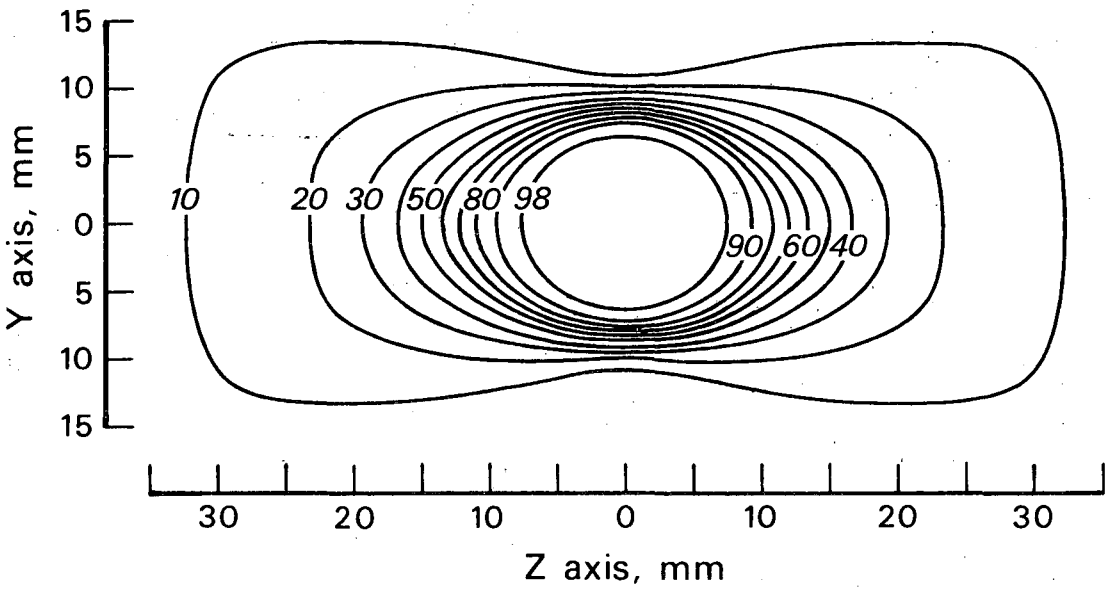

DBL 682-4579

Fig. 26. Isodose contours for a small ellipsoidal lesion produced by a 910-MeV helium ion beam, collimated by an 18×12-mm elliptical aperture, used for pituitary suppression.

Lesions of a more general form (ellipsoid) can be produced by rotation simultaneously about two perpendicular axes both of which are perpendicular to the beam axis. Isodose contours for such an irradiation are shown in Fig. 26. Such a technique has been in routine use at the 184-inch synchrocyclotron in Berkeley for the suppression of pituitary function (Lawrence and Tobias, 1965).

ACKNOWLEDGMENTS

The authors' work was generously supported by the U. S. Atomic Energy Commission, National Aeronautics and Space Administration, Office of Naval Research, and The Royal Norwegian Council for Technical and Industrial Research.

The authors are grateful to H. Bichsel for helpful suggestions, and to A. M. Koehler for helpful discussions and for his permission to use unpublished material. The authors take pleasure in thanking H. Aceto, D. K. Bewley, S. B. Curtis, J. F. Fowler, J. Howard, D. D. Love, H. D. Maccabee, C. J. Parnell, P. W. Todd, and C. P. Welch for helpful suggestions.

References

Aamodt, R. L., Peterson, V., and Phillips, R. (1952). $^{12}C(p,pn)^{11}C$ cross section from threshold to 340 MeV. Phys. Rev. 88, 739.

Barendsen, G. W., Walter, H. M. D., Fowler, J. F., and Bewley, D. K. (1963). Effects of different ionizing radiations on human cells in tissue culture. III. Experiments with cyclotron-accelerated alpha-particles and deuterons. Radiation Res. 18, 106.

Barkas, W. H., and Berger, M. J. (1964). Tables of energy losses and ranges of heavy charged particles. Studies in penetration of charged particles in matter. Natl. Acad. Sci.-Natl. Res. Council, Publ. 1133.

Bethe, H., and Ashkin, J. (1953). Passage of heavy particles through matter. In "Experimental Nuclear Physics" (E. Segrè, ed.), Vol. 1, p. 166. Wiley, New York.

Bewley, D. K., Field, S. B., and Parnell, C. J. (1967). Physical aspects of the deuteron and helium nuclei beams from the M. R. C. cyclotron. Phys. Med. Biol. 12, 1.

Bichsel, H. (1963). Passage of charged particles through matter. In "American Institute of Physics Handbook" (D. E. Gray et al., eds.), 2nd ed., pp. 8020. McGraw-Hill, New York.

Bichsel, H. (1967). A Fortran program for the calculation of the energy loss of heavy charged particles. Lawrence Radiation Lab. Rept. UCRL-17538.

Birge, A. C., and Sayeg, J. A. (1959). The effects of accelerated carbon nuclei and other radiations on the survival of haploid yeast. Radiation Res. 10, 433.

Blosser, T. V., Maienschein, F. C., and Freestone, R. M., Jr. (1964). The energy deposition in a water-filled spherical phantom by secondaries from high-energy protons and by neutrons. Health Phys. 10, 743.

Bobkov, V. G., Demin, V. P., Keirim-Markus, I. B., Kovalev, E. E., Larichiv, A. V., Sakovich, V. A., Smirennyy, L. N., and Sychkov, M. A. (1964). Radiation safety during space flights. NASA, Tech. Transl. F356.

Born, J. L., Anderson, A. O., Anger, H. O., Birge, A. C., Blanquet, P., Brustad, T., Carlson, R. A., Van Dyke, D. C., Fluke, D. J., Garcia, J., Henry, J. P., Knisely, R. M., Lawrence, J. H., Riggs, C. W., Thorell, B., Tobias, C. A., Toch, P., and Welch, G. P., (1959). Biological and medical studies with high-energy particle accelerators. Progr. Nucl. Energy, Ser. VII, 2, 189.

Brustad, T., (1961). Molecular and cellular effects of fast charged particles. Radiation Res. 15, 139.

Brustad, T., and Fluke, D. J. (1958). Effect of stripped carbon and oxygen ions in lysozyme. Radiation Res. 9, 95.

Brustad, T., Ariotti, P., and Lyman, J. T. (1960). Experimental setup and dosimetry for investigating biological effects of densely ionizing radiations. Lawrence Radiation Lab. Rep. UCRL-9454.

Chamberlain, O., Segrè, E., and Wiegand, C. (1951). Experiments on proton-proton scattering from 120 to 345 MeV. Phys. Rev. 83, 923.

Cumming, J. B. (1963). Monitor reactions for high energy proton beams. Ann. Rev. Nucl. Sci. 13, 26.

Dolphin, G. W., and Hutchinson, F. (1960). The actions of fast carbon and heavier ions on biological materials. I. The inactivations of dried enzymes. Radiation Res. 13, 403.

Engstrom, A., and Lindstrom, B. (1958). The weighing of cellular structure by ultra-soft x-rays. Gen. Cytochem. Methods 1, 1.

Fano, U. (1963). Penetration of protons, α particles and mesons. Ann. Rev. Nucl. Sci. 13, 1; reprinted in Natl. Acad. Sci.-Natl. Res. Council, Publ. 1133 (1964).

Fleischer, R. L., Price, P. B., and Walker, R. M., (1965). Tracks of charged particles in solids. Science 149, 383.

Fowler, P. H., and Perkins, D. H. (1961). Possibility of therapeutic applications of beams of negative π-mesons. Nature 189, 524.

Gooding, T. J., and Eisberg, R. M. (1957). Statistical Fluctuations in energy losses of 37-MeV protons. Phys. Rev. 105, 357.

Gordon, H. S., and Behman, G. A. (1963). Particle accelerators. In "American Institute of Physics Handbook" (D. E. Gray et al., eds.), 2nd ed., pp. 8-168. McGraw-Hill, New York.

Goulding, F. S. (1965). Semiconductor detectors for nuclear spectrometry. Lawrence Radiation Lab. Rept. UCRL-16231.

Gray, L. H. (1961). Radiobiologic basis of oxygen as a modifying factor in radiation therapy. Am. J. Roentgenol., Radium Therapy Nucl. Med. 85, 803.

Greening, J. R. (1954). A contribution to the theory of ionization chamber measurements at low pressure. Brit. J. Radiol. 27, 1963.

Grew, G. (1965). Cyclotron tests to determine the response of solid-state detectors to protons of energies 50 to 160 MeV for use in a proton spectrometer. IEEE, trans. Nucl. Sci. 12, No. 1, 308.

Hanna, R. C., and Hodges, T. A. (1965). A differential ion chamber for beam energy measurement. Nucl. Instr. Methods 37, 346.

Haynes, R. H., and Dolphin, G. W. (1959). The calculation of linear energy transfer, with special reference to a 14 MeV electron beam and 10 MeV per nucleon ion beams. Phys. Med. Biol. 4, 148.

Heckman, H. H., Perkins, B. L., Simon, W. G., Smith, F. M., and Barkas, W. H. (1960). Ranges and energy-loss processes of heavy ions in emulsion. Phys. Rev. 117, 544.

Henrikson, T. (1966). Production of free radicals in solid biological substances by heavy ions. Radiation Res. 27, 676.

Howard-Flanders, P. (1958). Physical and chemical mechanisms in the injury of cells by ionizing radiations. Advan. Biol. Med. Phys. 8, 553.

Hubbard, E. L. (1961). Heavy ion accelerators. Ann. Rev. Nucl. Sci. 2, 419.

Hubbard, E. L., and MacKenzie, K. R. (1952). The range of 18 MeV protons in aluminum. Phys. Rev. 85, 107.

Hubbard, E. L., Baker, W. R., Ehlers, K. W., Gordon, H. S., Main, R. M., Norris, N. J., Peters, R., Smith, L., Van Atta, C. M., Voelker, F., Anderson, C. E., Beringer, R., Gluckstron, R. L., Knon, W. J., Malkin, M. S., Quinton, A. R., Scharcz, L., and Wheeler, G. W. (1961). Heavy-ion linear accelerator. Rev. Sci. Instr. 32, 621.

ICRU (1962). Radiation quantities and units. Report 10a of the International Commission on Radiological Units and Measurements. Natl. Bur. Std. (U.S.) Handbook 84.

Jackson, H. G., Mack, D. A., and Wiegand, C. (1959). Beam profile indicator. IRE, Trans. Nucl. Sci. 6, 64.

Janni, J. F. (1966). Calculations of energy loss, range, path length, straggling, multiple scattering, and the probability of inelastic nuclear collisions for 0.1 to 1000-MeV protons. Air Force Weapons Lab. AFWL-TR 65-150.

Janssen, P., Klatzo, I., Miquel, J., Brustad, T., Behar, A., Haymaker, W., Lyman, J. T., Henry, J., and Tobias, C. A. (1962). Pathologic changes in the brain from exposure to alpha particles from a 60 inch cyclotron. In "Response of the Nervous System to Ionizing Radiation" (T. I. Haley and R. S. Snider, eds.), p. 383. Academic Press, New York.

Jung, H. (1967). Effects of protons on enzymes. Radiation Res. Suppl. 7, 164.

Karlsson, B. G. (1964). Methodern zur Berechnung und Erzielung Einigenfundie Tiefentherapie mit Hochenergetischen Protonen gunstiger Dosisverteilungen. Strahlentherapie 124, 481.

Kjellberg, R. N., Koehler, A. M., Preston, W. M., and Sweet, W. H. (1963). Biological and clinical studies using Bragg peak of proton beam. Proc. 2nd Intern. Congr. Radiation Res., Harrogate, England, 1962. North-Holland Publ., Amsterdam.

Kjellberg, R. N., Koehler, A. M., Preston, W. M., and Sweet, W. H. (1964). Intracranial lesions made by the Bragg peak of a proton beam. In "Response of the Nervous System to Ionizing Radiation" (T. J. Haley and R. S. Snider, eds.), p. 36. Little, Brown, Boston, Massachusetts.

Koehler, A. M. 1967a. Dosimetry of proton beams using small silicon diodes. Radiation Res. Suppl. 7, 53.

Koehler, A. M. (1967b). Private communication.

Landau, L. (1944). On the energy loss of fast particles by ionization J. Phys. USSR 8, 201.

Larsson, B. (1961). Pre-therapeutic physical experiments with high energy protons. Brit. J. Radiol. 34, 1943.

Larsson, B., Leksell, L., Rexed, B., Sourander, P., Mair, W., and Andersson, B. (1958). The high energy proton beam as a neurosurgical tool. Nature 182, 1222.

Larsson, B., Leksell, L., and Rexed, B. (1962). The use of high energy protons for cerebral surgery in man. Acta Chir. Scand. 125, 1.

Lawrence, J. H., and Tobias, C. A. (1965). Heavy particles in medicine. Progr. At. Med. 1, 127.

Lea, D. E. (1946). "Actions of Radiation on Living Cells." Cambridge-Univ. Press, London and New York.

Lea, D. E. (1955). "Action of Radiation on Living Cells," 2 ed. Cambridge Univ. Press, London and New York.

Leksell, L., Larsson, B., Andersson, B., Rexed, B., Sourander, P., and Mair, W. (1960). Lesions in the depth of the brain produced by a beam of high energy protons. Acta Radiol. 54, 251.

Lindhard, J. (1964). Thomas-Fermi approach and similarity in atomic collisions. Studies in penetration of charged particles in matter. Natl. Acad. Sci.-Natl. Res. Council, Publ. 1133.

Litton, G. M. (1967). Program BRAGG--a Fortran-IV program for calculating Bragg curves and flux distributions. Lawrence Radiation Lab. Rept. UCRL-17391.

Litton, G. M., Wallace, R., and Tobias, C. A. (1967). Penetration of high energy heavy ions. Lawrence Radiation Lab. Rept. UCRL-17292.

Lyman, J. T. (1965). Dark recovery of yeast following ionizing radiations. Ph. D. Thesis. Lawrence Radiation Lab. Rept. UCRL-16030.

Lyman, J. T. (1967). Distribution of ionization in heavy-charged-particle tracks. Biomedical Studies with heavy ion beams. Lawrence Radiation Lab. Rept. UCRL-17357, p. 42.

Maccabee, H. D. (1966). Fluctuations of energy loss by heavy charged particles in matter. Ph. D. Thesis. Lawrence Radiation Lab. Rept. UCRL-16931.

Maccabee, H. D., and Raju, M. R. (1968). Ionization fluctuations in cells and thin dosimeters. Proc. 1st Intern. Symp. Biol. Interpretation of Dose from Accelerator Produced Radiation, Berkeley, 1967. U. S. Atomic Energy Commission, p. 221; also Lawrence Radiation Lab. Rept. UCRL-17465.

Maccabee, H. D., Raju, M. R., and Tobias, C. A. (1966). Fluctuations of energy loss in semiconductor detectors. IEEE, Trans. Nucl. Sci. 13, No. 3, 176.

McMillan, E. M. (1959). Particle accelerators. Exptl. Nucl. Phys. 3, 639.

Malis, L. I., Loevinger, R., Kruger, L., and Rose, J. E. (1957). Production of laminar lesions in the cerebral cortex by heavy ionizing particles. Science 126, 302.

Malis, L. I., Rose, J. E., Kruger, L., and Baker, C. P. (1962). Production of laminar lesions in cerebral cortex by deuteron irradiation. In "Response of the Nervous Systems to Ionizing Radiation" (T. J. Haley, and R. S. Snider, eds.), p. 359. Academic Press, New York.

Manney, T. R., Brustad, T., and Tobias, C. A. (1963). Effects of glycerol and anoxia on the radiosensitivity of haploid yeasts to densely ionizing particles. Radiation Res. 18, 374.

Measday, D. F. (1966). The $^{12}C(p,pn)^{11}C$ reaction from 50 to 160 MeV. Nucl. Phys. 78, 476.

Neary, G. J. (1965). Chromosome aberrations and the theory of R.B.E. I. General considerations. Intern. J. Radiation Biol. 9, 477.

Norman, A. 1967. Thermal spike effects in heavy ion tracks. Radiation Res. Suppl. 7, 33.

Northcliffe, L. C. (1960). Energy loss and effective charge of heavy ions in aluminum. Phys. Rev. 120, 1744.

Northcliffe, L. C. (1964). Passage of heavy ions through matter. Ann. Rev. Nucl. Sci. 13, 67; reprinted in Natl. Acad. Sci.-Natl. Res. Council, Publ. 1133 (1964).

Oda, N., and Lyman, J. T. (1967). Secondary electron distribution for heavy ions. Radiation Res. Suppl. 7, 20.

Palmieri, J. N., and Goloskie, R. (1964). Calibration of 30-cm Faraday cup. Rev. Sci. Instr. 35, 4023.

Pollard, E. (1953). Primary ionization as a test of molecular organization. Advan. Biol. Med. Phys. 3, 153.

Pollard, E. C., Guild, W. R., Hutchinson, F., and Setlow, R. B. (1955). The direct action of ionizing radiation on enzymes and antigens. Progr. Biophys. Biophys. Chem. 5, 72.

Powers, E. L., Lyman, J. T., and Tobias, C. A. (1967). Some effects of accelerated charged particles on bacterial spores. Intern. J. Radiation Res. (to be published).

Preston, W. M., and Koehler, A. M. (1968). The effects of scattering on small proton beams. (to be published.)

Pruitt, J. S. (1966). Secondary electron trajectories in a Faraday cup magnetic field. Nucl. Instr. Methods 39, 329.

Raju, M. R. (1966). The use of the miniature silicon diode as a radiation dose meter. Phys. Med. Biol. 11, 371.

Raju, M. R. (1967). Heavy particle studies with silicon detectors. Radiation Res. Suppl. 7, 43.

Raju, M. R., Lampo, E. J., Curtis, S. B., Sperinde, J. M., and Richman, C. (1967). Lithium drifted silicon detector used as a pulse dosimeter. IEEE, Trans. Nucl. Sci. 14, No. 1, 559.

Raju, M. R., Richman, C., and Curtis, S. B. (1968). A review of the Physical characteristics of pion beams. Lawrence Radiation Lab. Rept. UCRL-17441; Proc. 1st Intern. Symp. Biol. Interpretation of Dose from Accelerator Produced Radiation, Berkeley, 1967 U. S. At. Energy Comm. p. 349.

Richman, C., Aceto, H., Raju, M. R., and Schwartz, B. (1966). The radiotherapeutic possibilities of negative pions. Am. J. Roentgenol., Radium Therapy Nucl. Med. 96, 777.

Roll, P. G., and Steigert, E. E. (1960). Effective charge of heavy ions in various media. Phys. Rev. 120, 470.

Rosenzweig, W., and Rossi, H. H. (1963). NYO-10716. Columbia University, New York.

Rossi, B. (1952). "High-Energy Particles." Prentice-Hall, Englewood Cliffs, New Jersey.

Santoro, R. T. (1965). The space, time and energy distribution of the beam of the Harvard University synchrocyclotron. ORNL-3722. Oak Ridge Natl. Lab., Oak Ridge, Tennessee.

Santoro, R. T., and Peele, R. W. (1964). Measurement of the intensity of the proton beam of the Harvard University synchrocyclotron for

energy-spectral measurements of nuclear secondaries. ORNL-3505. Oak Ridge Natl. Lab., Oak Ridge, Tennessee.

Santoro, R. B., Bertrand, F. E., Love, T. A., and Peele, R. W. (1966). Beam energy measurements at the Oak Ridge isochronous cyclotron. ORNL-TM-1382. Oak Ridge Natl. Lab., Oak Ridge, Tennessee.

Sargent, T. W. (1962). Metabolic studies with ^{59}Fe, ^{47}Ca and ^{11}C in various diseases. Proc. Symp. Whole-body Counting, Vienna, 1961 p. 447. IAEA, Vienna.

Sayeg, J. A., Birge, A. C., Beam, C. A., and Tobias, C. A. (1959). The effects of accelerated carbon nuclei and other radiations on the survival of haploid yeast. II. Biological experiments. Radiation Res. 10, 449.

Schambra, P. E., Rauth, A. M., and Northcliffe, L. C. (1960). Energy loss measurements for heavy ions in Mylar and polyethylene. Phys. Rev. 120, 1758.

Segrè, E. (1964). "Nuclei and Particles." Benjamin, New York.

Seltzer, S., and Berger, M. (1964). Energy loss straggling of protons and mesons: Tabulation of the Vavilov distribution. Studies in penetration of charged particles in matter. Natl. Acad. Sci.-Natl. Res. Council, Publ. 1133, 187.

Snyder, W. S., and Neufeld, J. (1957). On the passage of heavy particles through tissue. Radiation Res. 6, 67.

Sperinde, J. M. (1967). Private communication.

Sternheimer, R. M. (1966). Density effect for the ionization loss of charged particles. Phys. Rev. 145, 247.

Steward, P. (1967). In Stopping power and range-energy data of heavy ions in nongaseous media. Biomedical studies with heavy ion beams. Lawrence Radiation Lab. Rept. UCRL-17357, p. 8.

Symon, K. R. (1952). Fluctuations in energy lost by high energy charged particles in passing through matter. Ph. D. Thesis, Harvard University, 1948; summarized in "High Energy Particles" (B. Rossi, ed.), p. 32. Prentice-Hall, Englewood Cliffs, New Jersey.

Tautfest, G. W., and Fechter, H. R. (1955). A nonsaturable high-energy beam monitor. Rev. Sci. Instr. 26, 229.

Tilbury, R. S. (1966). Activation analysis with charged particles. U. S. At. Energy Comm. NAS-NS 3110.

Timofeeff-Ressovsky, N. W., and Zimmer, K. G. (1947). "Das Trefferprinzip in der Biologie." Vol. 1. Biophysik. S. Hirzel, Leipzig.

Tobias, C. A. (1962). The use of accelerated heavy particles for production of radiolesions and stimulation in the central nervous system. In "Response of the Nervous System to Ionizing Radiation" (T. J. Haley and R. S. Snider, eds.), p. 325. Academic Press, New York.

Tobias, C. A., and Manney, T. (1964). Some molecular and cellular effects of heavily ionizing radiations. Ann. N. Y. Acad. Sci. 114, 16.

Tobias, C. A., and Todd, P. (1964). Analysis of the effects of high LET radiations on various strains of cells. Symp. Biol. Effects of Neutron and Proton Irradiations, Upton, N. Y., 1963 Vol. II, p. 410. IAEA, Vienna.

Tobias, C. A., and Todd, P. (1967). Heavy charged particles in cancer therapy. Nat. Cancer Inst. Monograph 24, 1.

Tobias, C. A., Anger, H. O., and Lawrence, J. H. (1952). Radiological use of high energy deuterons and alpha particles. Am. J. Roentgenol., Radium Therapy Nucl. Med. 67, 1.

Tobias, C. A., Roberts, J. E., Lawrence, J. H., Low-Beer, B. V. A., Anger, H. O., Born, J. L., McCombs, R., and Huggins, C. (1956). Irradiation hypophysectomy and related studies using 340 MeV protons and 190 MeV deuterons. Proc. Intern. Conf. Peaceful Uses At. Energy, Geneva, 1955 Vol. 10, p. 95. Columbia Univ. Press (I. D. S.), New York.

Tobias, C. A., Lawrence, J. H., Born, J. L., McCombs, R. K., Roberts, J. E., Anger, H. O. Low-Beer, B. V. A., and Huggins, C. B. (1958). Pituitary irradiation with high-energy proton beams--a preliminary report. Cancer Res. 18, 121.

Trower, W. P. (1966). High-energy particle data. Vols. I-IV. Lawrence Radiation Lab. Rept. UCRL-2426 Rev.

Turner, J. E., Zerby C. D., Woodyard, R. L., Wright, H. A., Kinney, W. E., Snyder, W. S., and Neufeld, J. (1964). Calculation of radiation dose from protons to 400 MeV. Health Phys. 10, 783.

Tym, R., Lyman, J. T., Weyand, R. W., Tobias, C. A., Yanni, N. W., Born, J. L., and Lawrence, J. H. (1965). Heavy particles and Parkinson's Disease. Donner laboratory, semi-annual report, biology and medicine. Lawrence Radiation Lab. Rept. UCRL-16613, p. 104.

Van Allen, J. A. (1961). Corpuscular radiations in space. Radiation Res. 14, 540.

Van Dyke, D. C., and Janssen, P. (1963). Removal of cerebral cortical tissue with negligible scar formation using a beam of high-energy particles. J. Neurosurg. 20, 289.

Van Dyke, D. C., Janssen, P., and Tobias, C. A. (1962). Fluorescein as a sensitive, semiquantitative indicator of injury following α-particle irradiation of the brain. In "Response of the Nervous System to Ionizing Radiation" (T. J. Haley and R. S. Snider, eds.), p. 369. Academic Press, New York.

Vavilov, P. V. (1957). Ionization losses of high-energy heavy particles, Zh. Experim. i. Teor. Fiz. 32, 920; Soviet Phys. JETP (English Transl.) 5, 749.

Walske, M. C. (1952). The stopping power of K-electrons. Phys. Rev. 88, 1283.

Walske, M. C. (1956). Stopping power of L-electrons. Phys. Rev. 101, 940.

Webber, W. R. (1963). An evaluation of the radiation hazard due to solar-particle events. D2-90469. Aero Space Division, Boeing Company, Seattle, Washington.

Webber, W. R. (1966). An evaluation of solar-cosmic-ray events during solar minimum. D2-84274-1. Space Science Group, Boeing Company, Seattle, Washington.

Welch, G. (1967). Private communication.

Whaling (1958). The energy loss of charged particles in matter. In "Handbuch der Physik," Vol. 34, p. 193.

Wheeler, R. V. (1966). Depth-dose for protons and pions from 1.0 to 10.0 BeV/c. Health Phys. 12, 653.

Williamson, C. F., Boujot, J. P., and Picard, J. (1966). Tables of range and stopping power of chemical elements for charged particles of energy 0.05 to 500 MeV. Rapport CEA-R3042. Centre D'Études Nucléaires De Saclay.

Wilson, R. R. (1946). Radiological use of fast protons. Radiology 47, 487.

Zimmer, K. G. (1966). Some unusual topics in radiation biology. Radiation Res. 28, 830.

Zirkle, R. E. (1952). Speculations on cellular actions of radiations. In "Symposium on Radiobiology" (J. J. Nickson, ed.), p. 333. Wiley, New York.

Zirkle, R. E., and Tobias, C. A. (1953). Effects of ploidy and linear energy transfer on radiobiological survival curves. Arch. Biochem. Biophys. 47, 282.

Notes

Mudundi R. Raju, from Southwest Center for Advanced Studies, Dallas, Texas, is guest scientist at Lawrence Radiation Laboratory, Berkeley.

Norsk Hydro's Institute for Cancer Research, the Norweigian Radium Hospital, Montebello, Oslo 3, Norway.

This report was prepared as an account of Government sponsored work. Neither the United States, nor the Commission, nor any person acting on behalf of the Commission:

A. Makes any warranty or representation, expressed or implied, with respect to the accuracy, completeness, or usefulness of the information contained in this report, or that the use of any information, apparatus, method, or process disclosed in this report may not infringe privately owned rights; or

B. Assumes any liabilities with respect to the use of, or for damages resulting from the use of any information, apparatus, method, or process disclosed in this report.

As used in the above, "person acting on behalf of the Commission" includes any employee or contractor of the Commission, or employee of such contractor, to the extent that such employee or contractor of the Commission, or employee of such contractor prepares, disseminates, or provides access to, any information pursuant to his employment or contract with the Commission, or his employment with such contractor.